Rapid distortion theory on transversely sheared mean flows of arbitrary cross section

M. E. Goldstein[1], S. J. Leib[2] & M. Z. Afsar[3]

[1]National Aeronautics and Space Administration, Glenn Research Centre, Cleveland OH 44135, USA

[2]Ohio Aerospace Institute, Cleveland, OH 44142 USA

[3]Strathclyde University, Department of Mechanical and Aerospace Engineering, 75 Montrose St. Glasgow, GI 1XJ, UK

This paper is concerned with Rapid Distortion Theory on transversely sheared mean flows that (among other things) can be used to analyze the unsteady motion resulting from the interaction of a turbulent shear flow with a solid surface. It expands on a previous analysis of Goldstein, Leib and Afsar (*J. Fluid Mech.* Vol. 824, pp. 477-51) that uses a pair of conservation laws to derive upstream boundary conditions for planar mean flows and extends these findings to transversely sheared flows of arbitrary cross section. The results, which turn out to be quite general, are applied to the specific case of a round jet interacting with the trailing edge of a flat plate and used to calculate the radiated sound field, which is then compared with experimental data taken at the NASA Glenn Research Center.

---

1. Introduction

Many engineering problems involve the interaction of turbulent shear flows with solid surfaces (Bilka et al, 2014; Tufts, Wang and Wang, 2018; Ross, 2009). Tufts, Wang and Wang (2018) used Large Eddy Simulation (LES) to study the sound generated by the interaction of an aerofoil with a turbulent shear layer and Ross (2009) measured the acoustic radiation from these flows. However, this type of interaction can also be studied analytically by using Rapid Distortion Theory (RDT).

RDT uses linearized equations to analyse rapid changes in turbulent flows such as those that occur when the flow interacts with a solid surface. It applies whenever the turbulence intensity is small and the length (or time) scale over which the changes take place is short compared to the length (or time) scale over which the turbulent eddies evolve (Batchelor & Proudman,1954; Hunt,1973; Goldsten,1978a, 1979a; and Sagaut & Cambon, 2018). When interpreted asymptotically, these assumptions imply, among other things, that it is possible to identify a distance/time that is very (infinitely) large on the scale of the interaction, but still small on the distance/time scale over which the turbulent eddies evolve. The RDT assumptions also imply that the resulting flow is inviscid and non-heat conducting and is, therefore, governed by the Linearized Euler Equations, i.e., the Euler equations linearized about an arbitrary, usually steady, solution to the full nonlinear equations— customarily referred to as the base flow. But these equations can sometimes be used even when the RDT assumptions are not satisfied (e.g. for the prediction of Mach wave radiation at relatively low supersonic Mach numbers). A more detailed discussion of the validity of RDT can be found in Hunt and Carruthers (1990) who also give some examples of the types of problems to which it can be applied.

RDT was originally developed to study incompressible, locally homogeneous turbulence (Tayor,1938; Batchelor and Proudman,1954; Moffatt, 1967; Xie et al,2017 and Sagaut & Cambon,2018) Extensions to non-homogeneous turbulence were developed by Hunt (1973) and by Goldstein (1978a, 1978b, 1979a, 1979b), who further extended the theory to include compressibility and thereby allowed it to be used in aeroacoustic applications. The locally homogeneous assumption obviates the need for an upstream boundary condition, but the focus of the present paper in on non-homogenous RDT, which usually provides a much more realistic representation of the turbulent interactions. Or more specifically, it is concerned with non-homogenous RDT on transversely sheared mean flows.

The general theory was developed in a series of papers by Goldstein (1978b, 1979b) who showed that the solutions to the latter class of RDT problems can be expressed in terms of the Rayleigh equation Green's function and two convected quantities that can be specified arbitrarily. Goldstein et al (2013a, 2017) showed that the pressure and transverse velocity fluctuations can be represented by a convolution product of the Rayleigh equation Green's function and one of the arbitrary convected quantities, which allowed them to represent the Fourier transforms of these quantities as the product of a space-time Fourier transform of the Green's function and the Fourier transform of the convected quantity. They used this result to predict the acoustic spectrum of the sound produced by the interaction of a planar jet with the trailing edge of a flat plate and thereby established the applicability of RDT to this problem (which was only partially done in earlier work by Goldstein, 1979b and Olsen and Boldman, 1979). The low-frequency, Fourier--transformed --Green's function--which turns out to be independent of the mean flow velocity profile for the zero mean surface velocity case considered in that reference--was used to calculate the acoustic field, since the experiments show that most of the sound is generated at low frequencies. (The RDT analysis remains valid at low frequencies because, as noted above, the RDT assumptions ensure the existence of a time scale that is large compared to the scale of the interaction but still small relative to the decay time of the turbulent eddies.) One of the purposes of this paper is to extend these ideas to jets of arbitrary cross section and use the results to predict the noise radiated by a round jet interacting with the trailing edge of a flat plate.

An important consequence of the disparate length scales is that boundary conditions can be imposed in a region that lies infinitely far upstream on the scale of the interaction but is still close to the interaction site on the evolution scale of the undisturbed turbulence. The two arbitrary convected quantities, which do not decay at upstream infinity, can, therefore, be determined from these upstream conditions.

However, a major problem with this is that these quantities do not correspond to physically measurable variables, which must decay at large upstream distance when calculated from RDT. But Goldstein et al (2017) showed that appropriate gradients of these variables do not decay at upstream infinity and used this finding to relate these gradients to the arbitrary connected quantities and thereby developed physically realizable upstream boundary conditions for planar mean flows.

The present paper extends these findings to transversely sheared mean flows of arbitrary cross section, uses the results to relate the pressure spectrum to the second order turbulent velocity spectrum at upstream infinity and develops an appropriate model for the latter quantity. The results show that the streamwise Fourier transform of the low frequency Green's function is again independent of the mean velocity profile for a large class of zero surface velocity mean flows with non-planar cross sections. This means that the low frequency Green's function is the same as the low-frequency limit of the zero-mean

flow Green's function, which can frequently be computed by using well-known standard techniques (Noble, 1958).

The final formula is used it to predict the sound field produced by a circular jet interacting with the trailing edge of a semi-infinite flat plate. But this result is quite general and is expected to apply to any sufficiently localized flow configuration (such as the multiple jet configuration shown in figure 1) whose velocity field can be represented by level surfaces in an appropriate orthogonal coordinate system.

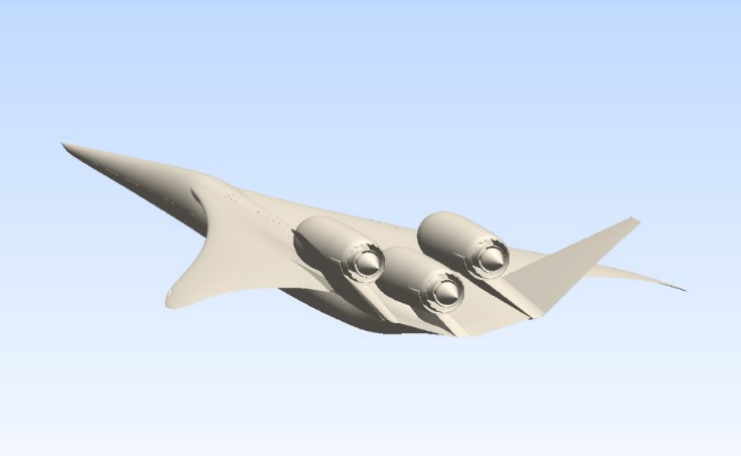

Figure 1 Supersonic cruse concept aircraft with top mounted engines. Ramakrishnan et al NASA CR-2018-219936 (photo provided by Dr. James Bridges)

Linear theories have also been used to study shock-turbulence interactions and are often referred to as Linear Interaction Approximations (LIA) in this context (see for example, Ribner, 1953; Moore, 1954; Woushuk *et al*. , 2009; Huete et al. 2010 ,2011 and 2012, as well as an extensive discussion of the subject by Saguat & Cambon (2018)). Compressible RDT and LIA share some common features (Huete Ruiz de Lira, 2010, 2011, 2012 and others). For example, both approaches decompose the flow into hydrodynamic and non- hydrodynamic components and both use transform methods to eliminate the time dependence.

Similar types of linear analyses are also used in fields beyond fluid mechanics and acoustics, such as astrophysics. The monograph by Sagaut and Cambon (2018) contains a comprehensive discussion of these analyses and of their application to a wide range of problems in physics and engineering.

A pseudo-linear approach called resolvent analysis, which was originally developed to study wall turbulence (see McKeon & Sharma 2010), has recently been used to predict the noise generation from turbulent flows. This approach decomposes the problem into forcing and response modes and seeks to determine dominant source modes for the development of reduced-order models of the sound field. An example of its application to the trailing-edge problem is given in Abreu et al. (2019).

The outline of the paper is as follows: It begins in section 2 by summarizing and reformulating the results obtained in Goldstein et al (2013a) for the formal solution to the complete inhomogeneous RDT problem.

Formulas are written down for the pressure fluctuation and a kind of particle displacement, both of which depend on one of the convected quantities alluded to above. These quantities are related by a conservation law which was originally derived in Goldstein (1979b) and in Goldstein et al (2013b) and rearranged into a more convenient form in the present paper.

The solutions are Fourier transformed in section 3 and the results are used in section 4 to obtain specific formulae for the pressure and particle displacement spectra, which are then combined with a result obtained in Goldstein et al (2017) to show that the pressure fluctuations and particle displacement drop out of the conservation law at upstream infinity where the flow is uninfluenced by the solid surface interaction. This result is then used to obtain an upstream boundary condition that relates the unknown convected quantity (or more specifically its spectrum) to the experimentally measurable transverse velocity spectrum and a parametrised model for this quantity is introduced. The low-frequency Green's function is discussed in section 5 and a generic--but incomplete--formula for its Fourier transform is derived for flow configurations that can be conformally mapped into a doubly infinite strip.

The specific case of an arbitrary cross section jet or shear layer interacting with the trailing edge of a flat plate is discussed in section 6 and an explicit solution for the Green's function is given in this case. As already mentioned this result turns out to be independent of the mean velocity profile and is therefore the same as the low frequency limit of the zero mean flow Green's function, which can frequently be calculated by well-known classical methods. We expect this finding to be quite generic and to apply to many low frequency transversely sheared RDT problems.

The Green's function solution is substituted into the formula for pressure fluctuation which is then used to obtain a relatively simple expression for the far field acoustic spectrum. And finally, this result is used in section 7 to obtain numerical predictions of the radiated sound field. The higher frequency predictions are greatly improved when the $O(1)$ frequency zero-mean-flow Fourier transformed Green's function is used in place of its low-frequency approximation. Some concluding remarks are given in Section 8.

2. Basic equations

The flow is assumed to be inviscid and non-heat conducting and the fluid is assumed to be an ideal gas so that the entropy is equal to $c_v \ln\left(p/\rho^{\gamma}\right)$ and the squared sound speed is equal to $\gamma p/\rho$, where p denotes the pressure, ρ the density, γ the specific heat ratio c_p/c_v, and c_p, c_v are the specific heats at constant pressure and volume respectively. Then the pressure $p' = p - p_0$ and mass flow (or density weighted velocity) perturbations

$$\boldsymbol{u} = \{u_1, u_2, u_3\} \equiv \rho\{v_1', v_2', v_3'\} \tag{2.1}$$

(where $\boldsymbol{v}' = \{v_1', v_2', v_3'\}$ denotes the velocity perturbation and $\rho = \rho(\boldsymbol{y}_T)$ denotes the mean density)on a transversely sheared mean flow with mean pressure p_0 =constant, velocity $\boldsymbol{v} = \{U(\boldsymbol{y}_T), 0, 0\}$ and mean sound speed squared $c^2(\boldsymbol{y}_T)$, decouple from the entropy fluctuations and are governed by the linearized momentum and continuity equations

$$\frac{D_0 u_i}{D\tau}+\delta_{1i}u_j\frac{\partial U}{\partial y_j}+\frac{\partial}{\partial y_i}p'=0,\quad i=1,2,3 \tag{2.2}$$

and

$$\frac{D_0 p'}{D\tau}+\frac{\partial}{\partial y_j}c^2 u_j=0\,, \tag{2.3}$$

where $D_0/D\tau \equiv \partial/\partial\tau + U\partial/\partial y_1$ is the convective derivative and, $\boldsymbol{y}=\{y_1,y_2,y_3\}=\{y_1,\boldsymbol{y}_T\}$ with y_1 in the streamwise direction and $\boldsymbol{y}_T=\{y_2,y_3\}$.

Goldstein et al (2013a) show that the pressure fluctuation p' produced at the observation point $\boldsymbol{x}=\{x_1,x_2,x_3\}$ by the interaction of the arbitrary convected disturbance $\tilde{\omega}\left(\tau - y_1/U(\boldsymbol{y}_T),\boldsymbol{y}_T\right)$ with any mean-flow-aligned solid surface embedded in this flow is given by

$$p'(\boldsymbol{x},t)=\int_{-T}^{T}\int_V G(\boldsymbol{y},\tau\,|\,\boldsymbol{x},t)\,\tilde{\omega}\left(\tau-\frac{y_1}{U(\boldsymbol{y}_T)},\boldsymbol{y}_T\right)d\boldsymbol{y}d\tau. \tag{2.4}$$

where $\tilde{\omega}\left(\tau - y_1/U(\boldsymbol{y}_T),\boldsymbol{y}_T\right)$ can be specified as an upstream boundary condition and $G(\boldsymbol{y},\tau\,|\,\boldsymbol{x},t)$ denotes the Green's function that satisfies the inhomogeneous Rayleigh equation

$$L\,\mathrm{G}(\boldsymbol{y},\tau\,|\,\boldsymbol{x},t)=\frac{D_0^3}{Dt^3}\delta(\boldsymbol{y}-\boldsymbol{x})\delta(\tau-t) \tag{2.5}$$

where

$$L\equiv\frac{D_0}{D\tau}\left(\frac{\partial}{\partial y_i}c^2\frac{\partial}{\partial y_i}-\frac{D_0^2}{D\tau^2}\right)-2\frac{\partial U}{\partial y_j}\frac{\partial}{\partial y_1}c^2\frac{\partial}{\partial y_j} \tag{2.6}$$

is the well-known compressible Rayleigh operator. The first two arguments of $G(\boldsymbol{y},\tau\,|\,\boldsymbol{x},t)$ represent the dependent variables and the second two represent the source variables, T denotes a very large but finite time interval, V is a region of space bounded by cylindrical (i.e., parallel to the mean flow) surface(s) S that can be finite, semi-infinite or infinite in the streamwise direction and $\hat{\boldsymbol{n}}=\{\hat{n}_i\}$ is the outward-drawn unit normal to S.

The operator

$$\frac{D_0}{Dt}\equiv\frac{\partial}{\partial t}+U(\boldsymbol{x}_T)\frac{\partial}{\partial x_1} \tag{2.7}$$

denotes the convective derivative in the $\boldsymbol{x}$ coordinate system, and $G(\boldsymbol{y},\tau\,|\,\boldsymbol{x},t)$ satisfies the boundary condition

$$\Lambda(\boldsymbol{y},\tau\,|\,\boldsymbol{x},t)=0\quad\text{for}\,\boldsymbol{y}\in S, \tag{2.8}$$

where Λ is determined to within an arbitrary convected quantity by

$$\frac{D_0^2\Lambda(\boldsymbol{y},\tau\,|\,\boldsymbol{x},t)}{D\tau^2}\equiv\hat{n}_j c^2\frac{\partial G(\boldsymbol{y},\tau\,|\,\boldsymbol{x},t)}{\partial y_j}, \tag{2.9}$$

on any solid (impermeable)surfaces S that are present in the flow, along with the jump conditions

$$\Delta[G] = \Delta[\Lambda] = 0, \quad \text{for } \boldsymbol{y}_T \in S_0 \tag{2.10}$$

across any surfaces S_0 of discontinuity of the mean velocity profile that may be present in the flow. The notation $\Delta[\square$ denotes the jump in the indicated quantity across these surfaces, which can represent downstream wakes (or vortex sheets) and can support spatially growing instability waves that can be generated by imposing a Kutta condition at the trailing edge or suppressed by imposing a boundedness requirement. It is worth noting that the analysis is somewhat unconventional in that the direct Green's function, G , now plays the role of an adjoint Green's function in the solution (2.4) for p' (Goldstein, Afsar and Leib, 2017).

The results given in Goldstein (1979b) and Goldstein et al (2013a, 2017) show that the mean density-weighted velocity perturbation u_i is given in terms of the mean-density-weighted pseudo-velocity perturbation

$$\tilde{\imath} \qquad \frac{D}{D\tau} \qquad -\delta_{1i}\frac{\partial U}{\partial y_j}\lambda_j, \quad \text{for } i = 1,2,3 \tag{2.11}$$

by

$$u_i = \tilde{\imath} \qquad \frac{1}{c^2}\frac{\partial U}{\partial y_j}\frac{\partial}{\partial y_k}\vartheta\left(\tau - \frac{y_1}{U}, \boldsymbol{y}_T\right), \tag{2.12}$$

where $\vartheta(\tau - y_1/U, \boldsymbol{y}_T)$ is a second arbitrary convected quantity and the 'particle displacement' λ_i is given by

$$\lambda_i = -\int_{-T}^{T}\int_V \tilde{C}_i(\ldots, t)\tilde{\ } \left(\qquad \frac{y_1}{U(\boldsymbol{y}_T)}, \boldsymbol{y}_T \right) d\boldsymbol{y}d\tau, \quad \text{for } i = 1,2,3 \tag{2.13}$$

with $\tilde{C}_i(\ldots, t)$ determined in terms of the Green's function derivative $\partial G(\boldsymbol{y}, \tau | \boldsymbol{x}, t)/\partial x_i$ of $G(\boldsymbol{y}, \tau | \boldsymbol{x}, t)$ by

$$\frac{D_0^2}{Dt^2}\tilde{C}_i(\ldots, t) = \frac{\partial}{\partial x_i}G(\boldsymbol{y}, \tau | \boldsymbol{x}, t), \quad \text{for } i = 1,2,3 \tag{2.14}$$

Equation(2.12) shows that mean-density-weighted transverse velocity perturbation $u_\perp$ and the divergence of the velocity perturbation can be determined from the mean-density-weighted-pseudo-velocity perturbation $\tilde{\imath}$ by

$$u_\perp \equiv \frac{1}{|\nabla U|}\frac{\partial U}{\partial y_i}u_i = \frac{1}{|\nabla U|}\frac{\partial U}{\partial y_i}\tilde{\imath}. \tag{2.15}$$

and

$$\frac{\partial c^2 u_i}{\partial y_i} = \frac{\partial c^2 \tilde{\imath}}{\partial y_i}. \tag{2.16}$$

Goldstein et al (2013b) show that the arbitrary convected quantity $\tilde{\omega}_c(\boldsymbol{y},\tau \mid \boldsymbol{x},t) = \tilde{\omega}_c(\boldsymbol{y},\tau \mid U,\boldsymbol{y}_T)$ is related to the pressure, transverse particle displacement λ_j and $\tilde{\imath}$ by the conservation law

$$\frac{\partial}{\partial y_1}\left(\tilde{\omega}_c \frac{\partial N_i}{\partial y_j}\frac{\partial U}{\partial y_i}\lambda_j\right) = \frac{\partial}{\partial y_k}\left(\frac{\partial N_i}{\partial y_i}\frac{\partial \tilde{\imath}}{\partial y_k}\right) \tag{2.17}$$

where

$$\tilde{\omega}_c = \varepsilon_{ijk}\frac{\partial \tilde{u}_k}{\partial y_j} \tag{2.18}$$

is the mean-density-weighted vorticity based on the pseudo-velocity and

$$N_i \equiv \frac{c^2}{|\nabla U|^2}\frac{\partial U}{\partial y_i}, \tag{2.19}$$

denotes a scaled mean velocity gradient. Differentiating by parts and using the well-known tensor identity

$$\varepsilon_{jik}\varepsilon_{jlm} = \delta_{il}\delta_{km} - \delta_{im}\delta_{kl} \tag{2.20}$$

shows that equation (2.17)can also be written as

$$\frac{\partial}{\partial y_1}\left(\tilde{\omega}_c \frac{\partial N_i}{\partial y_i}\frac{\partial U}{\partial y_j}\lambda_j\right) = N_k\tilde{\omega}_c - \left(\frac{\partial N_i}{\partial y_i} - \frac{\partial N_i}{\partial y_k}\right)\frac{\partial \tilde{\imath}}{\partial y_i} \tag{2.21}$$

where

$$\tilde{\omega}_c(\boldsymbol{y},\tau \mid \boldsymbol{x},t) = \nabla^2\tilde{\imath} - \frac{\partial}{\partial y_k} \tag{2.22}$$

As noted in Goldstein et al (2013a, 2017), the present formalism can be thought of as a generalization of a result obtained by Orr (1907) for the small-amplitude, unsteady, two-dimensional motion on an incompressible flow with uniform mean shear, with the most important difference being that the arbitrary convected quantity, $\tilde{\omega}_c$, no longer corresponds to an actual physical variable.

There have been many attempts in the literature to decompose the small amplitude unsteady motion on non-uniform mean flows into acoustic and hydrodynamic components. But it is impossible to unambiguously decompose the unsteady motion on an arbitrary transversely sheared mean flow into such components. We can however identify a hydrodynamic component of the motion by requiring that it not radiate any sound at subsonic Mach numbers, with all the acoustic radiation being accounted for by the remaining non-hydrodynamic component. This can be accomplished by dividing the Rayleigh equation Green's function $G(\boldsymbol{y},\tau \mid \boldsymbol{x},t)$ that appears in the solution (2.4) into two components, say

$$G(\boldsymbol{y},\tau \mid \boldsymbol{x},t) = G^{(0)}(\boldsymbol{y},\tau \mid \boldsymbol{x},t) + G^{(s)}(\boldsymbol{y},\tau \mid \boldsymbol{x},t) \tag{2.23}$$

where $G^{(0)}(\boldsymbol{y},\tau\,|\,\boldsymbol{x},t)$ denotes a particular solution of Eq.(2.5) ,which can either be defined on all space or, be required to satisfy homogeneous boundary conditions on extensions of the bounding surfaces S that range from minus to plus infinity in the streamwise direction. This decomposition implies the decomposition

$$\tilde{G}_i(\boldsymbol{y},\omega\,|\,\boldsymbol{x},t) = \tilde{G}_i^{(0)}(\boldsymbol{y},\omega\,|\,\boldsymbol{x},t) + \tilde{G}_i^{(s)}(\boldsymbol{y},\omega\,|\,\boldsymbol{x},t) \tag{2.24}$$

of the Green's function derivative (2.14)and the decomposition

$$p'(\boldsymbol{x},t) = p'^{(0)}(\boldsymbol{x},t) + p'^{(s)}(\boldsymbol{x},t) \tag{2.25}$$

for the pressure fluctuation, where $p'^{(0)}(\boldsymbol{x},t)$, which is given by (2.4) and (2.5) with $G(\boldsymbol{y},\tau\,|\,\boldsymbol{x},t)$ replaced by $G^{(0)}(\boldsymbol{y},\tau\,|\,\boldsymbol{x},t)$ and, since there are no edges in this (streamwise-homogeneous) flow ,does not produce any acoustic radiation at subsonic Mach numbers. The corresponding solution can, therefore, be identified with the hydrodynamic component of the unsteady motion. The remaining 'scattered component' $G^{(s)}(\boldsymbol{y},\tau\,|\,\boldsymbol{x},t)$ of(2.23), satisfies the homogeneous Rayleigh's equation along with appropriate inhomogeneous boundary and jump conditions on the streamwise discontinuous surfaces S and S_0 and the corresponding 'scattered solution' $p'^{(s)}(\boldsymbol{x},t)$, therefore, accounts for all of the acoustic radiation.

The decomposition(2.24) also implies the decomposition

$$\lambda_i(\boldsymbol{x},t) = \lambda_i^{(0)}(\boldsymbol{x},t) + \lambda_i^{(s)}(\boldsymbol{x},t), \quad \tilde{i} \qquad \tilde{i} \tag{2.26}$$

for the transverse particle displacement $\lambda_i(\boldsymbol{x},t)$ and the mean-density-weighted pseudo-velocity perturbation $\tilde{i}$ where $\lambda_i^{(0)}(\boldsymbol{x},t)$ is given by (2.13) with $\tilde{G}_i(\boldsymbol{y},\omega\,|\,\boldsymbol{x},t)$ replaced by $\tilde{G}_i$.

3. The pressure spectrum

Taking the Fourier transform of equation (2.4), applying the definitions (2.23)-(2.25), using the convolution theorem and noting that G satisfies the inhomogeneous Rayleigh equation (2.5), and therefore depends on τ and t only in the combination $t-\tau$, shows that

$$\overline{p}^{(\sigma)}(\boldsymbol{x}:\omega) = (2\pi)^2 \int_{A_T} e^{i\omega x_1/U(\boldsymbol{y}_T)} \overline{\overline{G}}^{(\sigma)}(\boldsymbol{y}_T\,|\,\boldsymbol{x}:\omega,\omega/U(\boldsymbol{y}_T))\,\overline{\Omega}(\boldsymbol{y}_T,\omega)\,d\boldsymbol{y}_T, \quad \sigma = 0,s, \tag{3.1}$$

where A_T denotes the cross sectional area of the volume V, $\alpha(\boldsymbol{x}:\omega) = \lim_{T\to\infty} \alpha(\boldsymbol{x}:\omega;T)$ for $\alpha = \overline{p}', \overline{\Omega}$

$$\overline{p}^{(\sigma)}(\boldsymbol{x}:\omega,T) \equiv \frac{1}{2\pi} \int_{-T}^{T} e^{i\omega t} p'^{(\sigma)}(\boldsymbol{x},t)\,dt \quad \sigma = 0,s \tag{3.2}$$

$$\bar{\Omega}\left(\boldsymbol{y}_T:\omega,T\right)\equiv\frac{1}{2\pi}\int_{-T}^{T}e^{i\omega z}\tilde{\iota}_{\left(\quad,\quad,\quad\right)}\,lz, \tag{3.3}$$

and

$$\bar{\bar{G}}^{(\sigma)}\left(\boldsymbol{y}_T\,|\,\boldsymbol{x};k_1,\omega\right)\equiv\frac{1}{\left(2\pi\right)^2}\int_{-\infty}^{\infty}\int_{-\infty}^{\infty}e^{i\left[k_1\left(y_1-x_1\right)+\omega\left(t-\tau\right)\right]}G^{(\sigma)}\left(\boldsymbol{y},\tau\,|\boldsymbol{x},t\right)d\tau dy_1\quad\sigma=0,s \tag{3.4}$$

satisfy the Rayleigh equations

$$\mathcal{L}\,\bar{\bar{G}}^{(0)}=0,\quad\mathcal{L}\,\bar{\bar{G}}^{(s)}=\omega^2\frac{\delta\left(\boldsymbol{x}_T-\boldsymbol{y}_T\right)}{\left(2\pi\right)^2} \tag{3.5}$$

in which

$$\mathcal{L}\equiv\frac{\partial}{\partial y_j}\frac{c^2}{\left(k_1U/\omega-1\right)^2}\frac{\partial}{\partial y_j}+\omega^2\left[1-\frac{c^2\left(k_1/\omega\right)^2}{\left(k_1U/\omega-1\right)^2}\right]\quad j=2,3 \tag{3.6}$$

denotes the reduced Rayleigh operator and $\bar{\bar{G}}^{(0)}\left(\boldsymbol{y}_T\,|\,\boldsymbol{x}:\omega,k_1\right)$ is either defined on all space or is required to satisfy

$$\frac{\hat{n}_j}{\left[\omega-k_1U\left(\boldsymbol{y}_T\right)\right]^2}\frac{\partial}{\partial y_j}\bar{\bar{G}}^{(0)}\left(\boldsymbol{y}_T\,|\,\boldsymbol{x}:\omega,k_1\right)=0,\ \text{ for }\ \boldsymbol{y}_T\in C_T \tag{3.7}$$

where C_T denotes the bounding curve/curves that generate the doubly infinite surface/surfaces that extend S from $y_1=-\infty$ to $y_1=+\infty$. The streamwise homogeneous Green's function $\bar{\bar{G}}^{(0)}\left(\boldsymbol{y}_T\,|\,\boldsymbol{x}:\omega,k_1\right)$ will then depend on y_1 and x_1 only in the combination x_1-y_1 and we can, therefore, write

$$\bar{\bar{G}}^{(0)}\left(\boldsymbol{y}_T\,|\,\boldsymbol{x}:\omega,k_1\right)=\bar{\bar{G}}^{(0)}\left(\boldsymbol{y}_T\,|\,\boldsymbol{x}_T:\omega,k_1\right). \tag{3.8}$$

4. Upstream Boundary conditions

Taking the Fourier transform of equation(2.13), applying the definitions (2.23), (2.26) and (3.4) using the convolution theorem and recalling that $G^{(0)}$ depends on τ and t only in the combination $t-\tau$ shows that

$$\bar{\lambda}_i^{(0)}\left(\boldsymbol{x},\omega\right)=-\frac{\left(2\pi\right)^2}{i\omega}\int_{A_T}e^{i\omega x_1/U\left(\boldsymbol{y}_T\right)}\frac{U\left(\boldsymbol{y}_T\right)\bar{\bar{G}}_i^{(0)}\left(\boldsymbol{y}_T\,|\,\boldsymbol{x}_T:\omega,\omega/U\left(\boldsymbol{y}_T\right)\right)}{U\left(\boldsymbol{x}_T\right)-U\left(\boldsymbol{y}_T\right)}\bar{\Omega}\left(\boldsymbol{y}_T:\omega\right)d\boldsymbol{y}_T, \tag{4.1}$$

where

$$\bar{\lambda}_i^{(0)}\left(\boldsymbol{x},\omega\right) \equiv \lim_{T\to\infty}\frac{1}{2\pi}\int_{-T}^{T} e^{i\omega t}\lambda_i^{(0)}\left(\boldsymbol{x},t\right)dt \qquad (4.2)$$

and the Green's function $\bar{\bar{G}}_i^{(0)}\left(\boldsymbol{y}_T \mid \boldsymbol{x}_T : \omega, k_1\right)$ also depends on y_1 and x_1 only in the combination $x_1 - y_1$ and is, therefore, given by

$$\bar{\bar{G}}_i^{(0)}\left(\boldsymbol{y}_T \mid \boldsymbol{x}_T : \omega, k_1\right) \equiv \frac{1}{i\left(k_1 U\left(\boldsymbol{x}_T\right)-\omega\right)}\frac{\partial}{\partial x_i}\bar{\bar{G}}^{(0)}\left(\boldsymbol{y}_T \mid \boldsymbol{x}_T : \omega, k_1\right),\ i = 2,3 \qquad (4.3)$$

The integral in (4.1) has the same singularity as that in equation (4.13) of Goldstein et al (2017) (the corresponding the formula is for $\partial\bar{\lambda}_i^{(0)}\left(\boldsymbol{x},\omega\right)/\partial x_1$) which means that it has to be interpreted as a Cauchy principal value and the procedure used in Appendix C of that paper (which applies to any transversely sheared mean flow) can be applied to this equation to show that

$$\bar{\lambda}_i^{(0)}\left(\boldsymbol{x},\omega\right) \to \frac{e^{i\omega x_1/U(\boldsymbol{x}_T)}}{x_1}\bar{\mathcal{L}}_i\left(\boldsymbol{x}_T,\omega\right),\ \text{for } i = 2,3 \text{ as } x_1 \to -\infty \qquad (4.4)$$

when causality is imposed, which, in turn, implies that

$$\lambda_i^{(0)}\left(\boldsymbol{x},t\right) \to \frac{1}{x_1}\mathcal{L}_i\left(t - x_1/U\left(\boldsymbol{x}_T\right),\boldsymbol{x}_T\right),\ \text{for } i = 2,3 \ \text{ as } x_1 \to -\infty \qquad (4.5)$$

where the purely convected quantity $\mathcal{L}_i\left(t - x_1/U\left(x_2\right),\boldsymbol{x}_T\right)$ is a function of the indicated arguments and $\bar{\mathcal{L}}_i\left(\boldsymbol{x}_T,\omega\right)$ is its Fourier transform.

Inserting (4.5) into(2.11) shows that

$$\tilde{\imath}\ [illegible] \to \frac{1}{x_1^2}\tilde{\mathcal{U}}_i\ [illegible]\ U\left(\boldsymbol{x}_T\right),\boldsymbol{x}_T\right),\ \text{for } i = 2,3 \ \text{ as } x_1 \to -\infty \qquad (4.6)$$

and, therefore, that

$$\bar{\tilde{\imath}}\ [illegible]\ {}_{T\to\infty}\frac{1}{2\pi}\int_{-T}^{T}\ [illegible]\ \frac{e^{i\omega x_1/U(\boldsymbol{x}_T)}}{x_1^2}\bar{\mathcal{U}}_i\left(\boldsymbol{x}_T,\omega\right),\ \text{for } i = 2,3 \ \text{ as } x_1 \to -\infty \qquad (4.7)$$

where, $\tilde{\mathcal{U}}_i$ [illegible] $U\left(x_2\right),\boldsymbol{x}_T\right)$ and $\bar{\mathcal{U}}_i\left(\boldsymbol{x}_T,\omega\right)$ have the obvious meanings.

Inserting (4.6) into(2.12) and using the result in the momentum equation (2.2) shows that

$$\frac{\partial p'^{(0)}\left(\boldsymbol{x},t\right)}{\partial x_i} \to \frac{2}{x_1^3}U\left(\boldsymbol{x}_T\right)\tilde{\imath}\ [illegible]\ U\left(\boldsymbol{x}_T\right),\boldsymbol{x}_T\right),\ \text{as } x_1 \to -\infty,\ \text{for } i = 2,3 \qquad (4.8)$$

And it therefore follows from (4.5) and (4.6) that the conservation law (2.21)and (2.22) becomes

$$\frac{\partial \tilde{\imath}}{\partial y_1} \to N_k\ [illegible] \to -\infty \qquad (4.9)$$

where

$$\tilde{\Gamma}_{\kappa} \; \nabla^2 \tilde{\iota} \qquad \frac{\partial}{\partial y_k} \tag{4.10}$$

But using(2.16) and the continuity equation (2.3) in (4.10)shows that

$$\tilde{\Gamma}_{\kappa} \; \nabla^2 \tilde{\iota} \qquad \frac{\partial}{\partial y_k}\left[\quad \left(\frac{D \; p'^{(0)}}{D\tau} \qquad \frac{\partial c^2}{\partial y_j} \right)\right] \tag{4.11}$$

And it therefore follows from (4.6)and (4.8) that

$$\tilde{\Gamma}_{\kappa} \; \to \nabla_{\perp}^2 \tilde{\iota} \qquad = 2,3 \text{ as } y_1 \to -\infty \tag{4.12}$$

where

$$\nabla_{\perp}^2 \equiv \frac{\partial^2}{\partial y_2^2} + \frac{\partial^2}{\partial y_3^2} \tag{4.13}$$

Equations(2.15),(4.6),(2.19) (4.9) and (4.12) then imply that

$$\frac{\partial \tilde{\iota}}{\partial y_1} = \frac{}{|\nabla U|^2} \nabla_{\perp}^2 \left(\frac{\partial U}{\partial y_k} u_k^{(0)} \right) + \mathrm{O}\left(\frac{1}{y_1} \right) = \frac{c^2}{|\nabla U|^2} \nabla_{\perp}^2 \left[\frac{1}{y_1^2} \frac{\partial U}{\partial y_k} \mathcal{U}_k \left(\tau - y_1 / U, \boldsymbol{y}_T \right) \right] + \mathrm{O}\left(\frac{1}{y_1} \right)$$

$$\to \frac{c^2}{U^4} \frac{\partial U}{\partial y_k} \frac{\partial^2}{\partial \tau^2} \mathcal{U}_k \left(\tau - y_1 / U, \boldsymbol{y}_T \right), \text{ as } y_1 \to -\infty, \tag{4.14}$$

which shows, among other things, that $\tilde{\iota}$ can be expressed in terms of the hydrodynamic component $\boldsymbol{u}^{(0)}$ of the physical velocity $\boldsymbol{u}$ instead the hydrodynamic component of the pseudo-velocity $\tilde{\iota}$ at upstream infinity and thereby provides the required upstream boundary condition that relates $\tilde{\iota}$ to an actual physical quantity. Equation (4.14)can also be written as

$$\frac{\partial \tilde{\iota}}{\partial y_1} \to \frac{}{U^4} \frac{dU}{du} \frac{\partial^2}{\partial \tau^2} |\nabla u| \mathcal{U}_{\perp} \left(\tau - y_1 / U(u), \boldsymbol{y}_T \right), \text{ as } y_1 \to -\infty, \tag{4.15}$$

where

$$\mathcal{U}_{\perp} \equiv \frac{\partial u}{\partial y_k} \frac{\mathcal{U}_k}{|\nabla u|} \tag{4.16}$$

when the level surfaces of $U = U(u)$, say $u(\boldsymbol{y}_T) = \text{constant}$, are more or less concentric and form an orthogonal coordinate system with some function $v(\boldsymbol{y}_T)$; $u_{\perp}$ then denotes the velocity component perpendicular to these surfaces.

These equations imply that the upstream boundary condition (4.15)will be satisfied when $\bar{\Omega}(\boldsymbol{y}_T : \omega, T)$ is related to the Fourier transform

$$\bar{\mathcal{U}}_{\perp}(\boldsymbol{y}_T; \omega, T) \equiv \frac{1}{2\pi} \int_{-T}^{T} e^{i\omega\xi} \mathcal{U}_{\perp}(\xi, \boldsymbol{y}_T) d\xi \tag{4.17}$$

of the upstream transverse velocity coefficient $\mathcal{U}_\perp(\xi, \boldsymbol{y}_T)$ (in the, as yet, arbitrary orthogonal curvilinear co-ordinate system $\{u,v\}(\boldsymbol{y}_T)$) by

$$\frac{i\omega}{U}\bar{\Omega}(\boldsymbol{y}_T:\omega,T) = -\omega^2\frac{c^2}{U^4}|\nabla u|\frac{dU}{du}\bar{\mathcal{U}}_\perp(\boldsymbol{y}_T;\omega,T) \tag{4.18}$$

which determines the Fourier transform $\bar{\Omega}(\boldsymbol{y}_T:\omega,T)$ of [illegible], and therefore the unknown convected quantity [illegible] $U(\boldsymbol{y}_T), \boldsymbol{y}_T)$ itself, in terms of the Fourier transform $\bar{\mathcal{U}}_\perp(\boldsymbol{y}_T;\omega,T)$ of $\mathcal{U}_\perp(\xi,\boldsymbol{y}_T)$, which is related to the upstream limit of the physical variable $u_k^{(0)}$ by(4.14).

Since the focus of this paper is on fully developed turbulent flows it is reasonable to assume that the source function [illegible] is a stationary random function of τ (Pope, 2000; Wiener, 1938) and it then follows from equation (2.4) that the pressure fluctuation $p'(t,\boldsymbol{x})$ should also be a function of this type. The spectrum of the scattered component of the pressure fluctuation, which is usually of primary interest in aeroacoustics and structures problems is then given by (Weiner, 1938)

$$I_\omega(\boldsymbol{x}) \equiv \frac{1}{2\pi}\int_{-\infty}^{\infty} e^{i\omega\tilde{\tau}} \langle p'(\boldsymbol{x},t)\, p'(\boldsymbol{x},t+\tilde{\tau}) \rangle \, [\text{illegible}] \lim_{T\to\infty}\frac{\bar{p}^{(s)}(\boldsymbol{x}:\omega,T)\left[\bar{p}^{(s)}(\boldsymbol{x}:\omega,T)\right]^*}{2T} \tag{4.19}$$

where the $\langle\ \rangle$ bracket denotes the time average

$$\langle p'(\boldsymbol{x},\tau)\, p'(\boldsymbol{x},\tau+\tilde{\tau}) \rangle [\text{illegible}] \lim_{T\to\infty}\frac{1}{2T}\int_{-T}^{T} [\text{illegible}] \tag{4.20}$$

Inserting the solution (3.1) for the scattered component of the pressure fluctuation into (4.19) and using (4.18)shows that its spectrum depends on the turbulent fluctuations only through source spectrum

$$S(\boldsymbol{y}_T|[\text{illegible}]) [\text{illegible}] \frac{1}{2\pi}\int_{-\infty}^{\infty} [\text{illegible}] \lim_{T\to\infty}\frac{\bar{\Omega}(\boldsymbol{y}_T:\omega,T)\left[\bar{\Omega}([\text{illegible}])\right]^*}{2T}$$

$$= \omega^2\frac{c^2(\boldsymbol{y}_T)c^2([\text{illegible}])}{U^3(u)U^3([\text{illegible}])}[\text{illegible}]\frac{dU([\text{illegible}])}{d[\text{illegible}]}[\text{illegible}] \lim_{T\to\infty}\frac{\bar{\mathcal{U}}_\perp(\boldsymbol{y}_T;\omega,T)\left[\bar{\mathcal{U}}_\perp([\text{illegible}])\right]^*}{2T} \tag{4.21}$$

when the level surfaces of $U = U(u)$, say $u(\boldsymbol{y}_T) = \text{constant}$, are more or less concentric and form an orthogonal coordinate system with some function $v(\boldsymbol{y}_T)$.

The spectrum of the gradient-wise velocity coefficient $\lim_{T\to\infty}\bar{\mathcal{U}}_\perp(\boldsymbol{y}_T;\omega,T)\left[\bar{\mathcal{U}}_\perp([\text{illegible}])\right]^*/2T$ must be modelled in order to use this equation to predict the source spectrum S. An appropriate model for this quantity that is consistent with the transversely sheared model for the mean flow is given Appendix B. The results show that the corresponding model for the source spectrum is given by

$$S\left(u,\tilde{\iota} \;\; \tilde{\;} \;\; \right) \;\; \left[\frac{dU/du}{U^2(u)} \frac{dU/d\tilde{\iota}}{U^2(\tilde{\iota})} \right] \frac{1}{2\pi}\int_{-\infty}^{\infty} \; i\omega \;)\big]\big)$$

$$\times\exp$$

$$= l_2^4 A(u,v)\left(\rho_\infty c_\infty^2\right)^2 \left[\frac{dU/du}{U^2(u)} \frac{dU/d\tilde{\iota}}{U^2(\tilde{\iota})} \right] \frac{f}{\pi\sqrt{1+\tilde{\iota}}} K_1\left(f\sqrt{1+\tilde{\iota}}\right) \qquad (4.22)$$

where

$$\tilde{\iota} \qquad (4.23)$$

and K_1 denotes the modified Bessel function of the second kind.

5. The Fourier-transformed Green’s function

It is of course necessary to determine the Fourier transformed Green’s function before equation (3.1) can be used to carry out numerical computations. This must, in general, be done numerically and the calculations, which tend to be very sensitive to the boundary conditions, frequently require great care- especially when mean the flow is discontinuous downstream of the trailing edge and therefore contains shear layers that can support spatially growing instability waves. The Wiener-Hopf technique (Noble, 1958)] can often be used to minimize these difficulties, but numerical computations are in most cases still required. Baker and Peake (2019) developed efficient numerical algorithms for carrying these out these computations. However, as noted as noted in the introduction, the sound generated by the solid surface interactions turns out to be of low frequency in most applications of technological interest-- which means that the low frequency Green’s function can be used in the calculations. The required computations can often be facilitated by first mapping the transverse geometry of the problem into an appropriate rectangular region.

5.1 Conformal mapping

To this end we suppose, with little loss of generality, that the level surfaces of c^2 coincide with the level surfaces $u = \text{constant}$ introduced below(4.16) (i.e., $U = U(u)$ and $c^2 = c^2(u)$) and further restrict u and the orthogonal variable v by requiring that

$$W(z) = u(\boldsymbol{y}_T) + iv(\boldsymbol{y}_T) \qquad (5.1)$$

be an analytic function of the complex variable

$$z = y_3 + iy_2 \qquad (5.2)$$

that transforms the upper half z-plane into the strip, $-\infty < u < 0, -\pi \le v \le \pi,$ in the W-plane. (A specific example is given in Appendix A.) We also suppose that the impermeable surface S is infinitely thin.

Transforming the linear operator and delta functions in equations (3.5)and (3.6)leads to the following equation for $\bar{\bar{G}}\left(u,v\middle|\boldsymbol{x}:\omega,k_1\right) \equiv \bar{\bar{G}}\left(\boldsymbol{y}_T(u,v)\middle|\boldsymbol{x}:\omega,k_1\right)$

$$\mathcal{L}_W \,\overline{\overline{\overline{G}}}\left(u,v\middle|\boldsymbol{x}:\omega,k_1\right)=\left(\frac{\omega}{2\pi}\right)^2\delta\left(u\left(\boldsymbol{y}_T\right)-u\left(\boldsymbol{x}_T\right)\right)\delta\left(v\left(\boldsymbol{y}_T\right)-v\left(\boldsymbol{x}_T\right)\right) \tag{5.3}$$

where

$$\mathcal{L}_W \equiv \frac{\partial}{\partial u}\frac{c^2\left(u\right)}{\left[U\left(u\right)k_1/\omega-1\right]^2}\frac{\partial}{\partial u}+\frac{c^2\left(u\right)}{\left[U\left(u\right)k_1/\omega-1\right]^2}\frac{\partial^2}{\partial v^2}$$

$$+\omega^2\left|\frac{dW}{dz}\right|^{-2}\left\{1-\frac{c^2\left(u\right)\left(k_1/\omega\right)^2}{\left[U\left(u\right)k_1/\omega-1\right]^2}\right\}. \tag{5.4}$$

The appropriate boundary conditions for $\overline{\overline{\overline{G}}}$ are that it be periodic in v and remain bounded for all value of u.

The decomposition (2.23) now implies that

$$\overline{\overline{\overline{G}}}\left(u,v\,|\,\boldsymbol{x}:\omega,k_1\right)=\overline{\overline{\overline{G}}}^{(0)}\left(u,v\,|\,\boldsymbol{x}_T:\omega,k_1\right)+\overline{\overline{\overline{G}}}^{(s)}\left(u,v\,|\,\boldsymbol{x}:\omega,k_1\right). \tag{5.5}$$

And the scattered component of the Green's function can be expressed as the sum of its symmetric, $\left[\overline{\overline{\overline{G}}}^{(s)}\left(u,v\,|\,x_1,x_2,x_3:\omega,k_1\right)+\overline{\overline{\overline{G}}}^{(s)}\left(u,v\,|\,x_1,x_2,-x_3:\omega,k_1\right)\right]/2$, and antisymmetric, $\left[\overline{\overline{\overline{G}}}^{(s)}\left(u,v\,|\,x_1,x_2,x_3:\omega,k_1\right)-\overline{\overline{\overline{G}}}^{(s)}\left(u,v\,|\,x_1,x_2,-x_3:\omega,k_1\right)\right]/2$, parts, which we now consider separately. These quantities have the representation

$$\left[\overline{\overline{\overline{G}}}^{(s)}\left(u,v\,|\,x_1,x_2,x_3:\omega,k_1\right)\pm\overline{\overline{\overline{G}}}^{(s)}\left(u,v\,|\,x_1,x_2,-x_3:\omega,k_1\right)\right]/2$$

$$=\int_{-\infty}^{\infty}\frac{1}{2}\left(e^{ik_3x_3}\pm e^{-ik_3x_3}\right)\overline{\overline{\overline{G}}}^{(s)}\left(u,v\,|\,x_1,x_2:\omega,k_1,k_3\right)dk_3$$

$$=\int_{-\infty}^{\infty}e^{ik_3x_3}\overline{\overline{\overline{G}}}_{\pm}^{(s)}\left(u,v\,|\,x_1,x_2:\omega,k_1,k_3\right)dk_3 \tag{5.6}$$

where we have put

$$\overline{\overline{\overline{G}}}_{\pm}^{(s)}\left(u,v\,|\,x_1,x_2:\omega,k_1,k_3\right)\equiv\frac{1}{2}\left[\overline{\overline{\overline{G}}}^{(s)}\left(u,v\,|\,x_1,x_2:\omega,k_1,k_3\right)\pm\overline{\overline{\overline{G}}}^{(s)}\left(u,v\,|\,x_1,x_2:\omega,k_1,-k_3\right)\right] \tag{5.7}$$

and the three overbars denote the Fourier transform

$$\overline{\overline{\overline{G}}}^{(\sigma)}\left(u,v\,|\,x_1,x_2:\omega,k_1,k_3\right)\equiv\frac{1}{2\pi}\int_{-\infty}^{\infty}e^{-ik_3x_3}\overline{\overline{\overline{G}}}^{(\sigma)}\left(u,v\,|\,\boldsymbol{x}:\omega,k_1\right)dx_3 \tag{5.8}$$

for $\sigma=0,s$, where the hydrodynamic component

$$\overline{\overline{\overline{G}}}^{(0)}\left(u,v \mid x_1,x_2 : \omega,k_1,k_3\right) = \overline{\overline{\overline{G}}}^{(0)}\left(u,v \mid x_2 : \omega,k_1,k_3\right) \tag{5.9}$$

is independent of x_1 and satisfies the wall boundary condition

$$\frac{\partial \overline{\overline{\overline{G}}}^{(0)}\left(u,v \mid x_2 : \omega,k_1,k_3\right)}{\partial u} = 0, \quad \text{for } u = 0, \quad -\pi \le v \le \pi. \tag{5.10}$$

5.2. Solution for the low frequency Green's function

We now consider the low -frequency limit ω,k_1 □ , and assume that all lengths normalized by some characteristic length scale, such as the distance h between the nozzle centerline and the plate, all velocities by sound speed at infinity, say c_∞^*, and the time by h / c_∞^*. The solution then divides into two regions: an outer region where $k_1 y_2, k_1 y_3 = O(1)$ and an inner region where $y_3, y_3 = O(1)$.

Figure 2 shows how these regions are transformed into the u,v plane by a conformal mapping of the type (A.1). The unconventional asymptotic structure shown in Figure 2 (b) is consistent with equation (A.7) which implies that the mapping 'reverses' the usual orientation of the inner and outer regions in the u,v plane

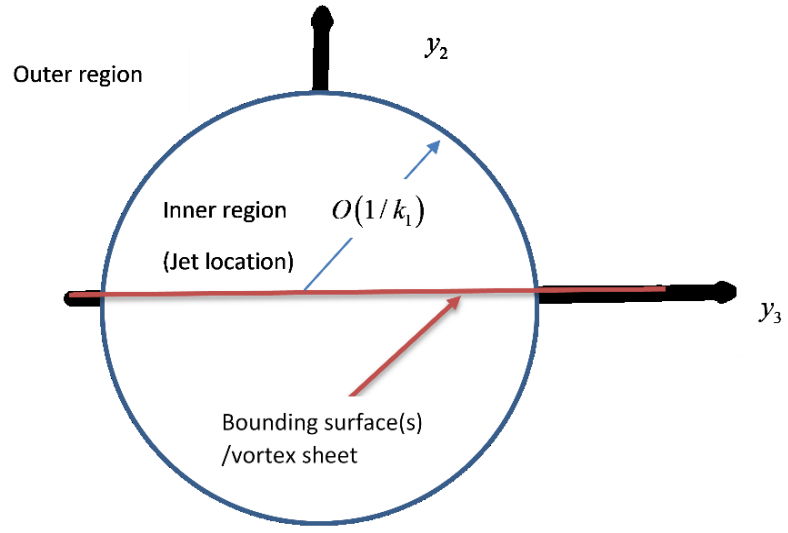

a)

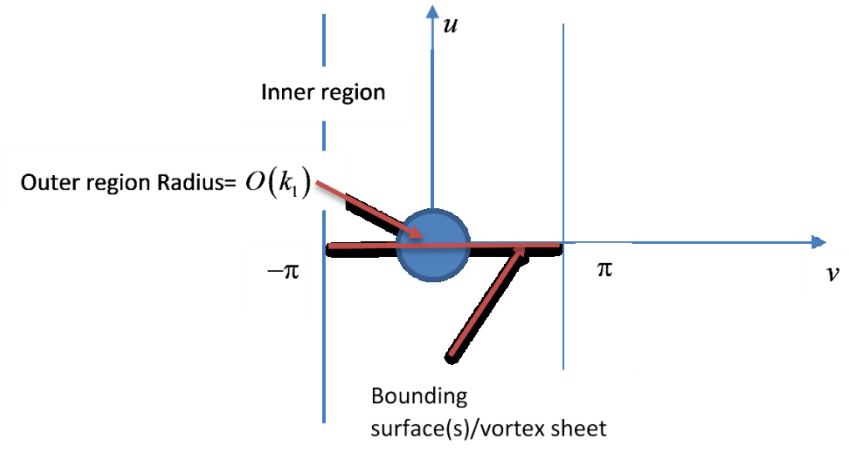

b)

Figure 2. Inner and outer regions for jet trailing edge interaction a) in $\boldsymbol{y}_T$ – plane, b) in W-plane.

Then since the delta function can always be set to zero when $v(\boldsymbol{y}_T) > v(\boldsymbol{x}_T)$, the lowest-order solutions (i.e. less than $O\left(k_\infty^2 - k_1^2 - k_3^2\right)$) can be obtained by replacing (5.3) and (5.8)with

$$\mathcal{L}_W \, \bar{\bar{\bar{G}}}^{(\sigma)}\left(u,v\middle|x_1,x_2:\omega,k_1,k_3\right)=0, \quad \sigma=0,s \tag{5.11}$$

for $v=O(1), k_\infty\left|\boldsymbol{x}_T\right|=O(1)$ and approximating $\mathcal{L}_W$ by

$$\mathcal{L}_W \approx \frac{\partial}{\partial u}\frac{c^2(u)}{\left[M(u)k_1/k_\infty-1\right]^2}\frac{\partial}{\partial u}+\frac{c^2(u)}{\left[M(u)k_1/k_\infty-1\right]^2}\frac{\partial^2}{\partial v^2}+O\left(k_\infty^2\right) \tag{5.12}$$

with

$$M(u)\equiv U(u)M_J, \quad k_\infty\equiv\omega M_J, \quad M_J\equiv U_J/c_\infty^*. \tag{5.13}$$

Multiplying (5.11) by e^{-inv} and integrating the result from $-\pi$ to π shows that

$$\bar{\bar{\bar{G}}}^{(\sigma)}\left(u,v\middle|x_1,x_2:\omega,k_1,k_3\right)=\sum_{n=-\infty}^{\infty}e^{inv}\bar{\bar{\bar{G}}}_n^{(\sigma)}\left(u\,|\,x_1,x_2:\omega,k_1,k_3\right), \quad \sigma=0,s \tag{5.14}$$

where

$$\bar{\bar{\bar{G}}}_n^{(\alpha)}\left(u\,|\,x_1,x_2:\omega,k_1,k_3\right)\equiv\frac{1}{2\pi}\int_{-\pi}^{\pi}e^{-inv}\bar{\bar{\bar{G}}}^{(\alpha)}\left(u,v\,|\,x_1,x_2:\omega,k_1,k_3\right)dv, \quad \alpha=0,s \tag{5.15}$$

satisfies the following infinite set of second order ordinary differential equations

$$\mathrm{L}_n \bar{\bar{\bar{G}}}_n^{(\alpha)}\left(u \mid x_1, x_2 : \omega, k_1, k_3\right) = 0 \tag{5.16}$$

where

$$\mathrm{L}_n \equiv \frac{d}{du}\frac{c^2(u)}{\left[M(u)(k_1/k_\infty)-1\right]^2}\frac{d}{du} - \frac{c^2(u)n^2}{\left[M(u)(k_1/k_\infty)-1\right]^2} + O\left(k_\infty^2\right) \tag{5.17}$$

and

$$\bar{\bar{\bar{G}}}_n^{(0)}\left(u \mid x_1, x_2 : \omega, k_1, k_3\right) = \bar{\bar{\bar{G}}}_n^{(0)}\left(u \mid x_2 : \omega, k_1, k_3\right). \tag{5.18}$$

The solution to (5.11) with $\sigma = s$ must match onto the spanwise Fourier transform of the outgoing wave outer solution, say $\bar{\bar{\bar{G}}}^{(s)}\left(\boldsymbol{y}_\perp \mid \boldsymbol{x}; k_1, \omega\right)$, which applies in outer the region where $x_T\sqrt{k_\infty^2 - k_1^2 - k_3^2}$. , $y_T\sqrt{k_\infty^2 - k_1^2 - k_3^2} = O(1)$. Equations (A.9)and (A.10) suggest that the solution in this region should be expressed in the rectangular coordinates y_2, y_3 and therefore satisfy the inhomogeneous Rayleigh equation (3.5) where $\mathscr{L}$ denotes the reduced Rayleigh operator (3.6) which can now be replaced by

$$\mathscr{L} = \frac{\partial^2}{\partial y_2^2} + \frac{\partial^2}{\partial y_3^2} + k_\infty^2 - k_1^2 \tag{5.19}$$

Appendix C shows that the lowest order inner solution for the Fourier transformed symmetric component of the Green's function that satisfies the wall boundary condition (2.8) for all values of y_3 is given by

$$\frac{1}{2}\left[\bar{\bar{\bar{\mathrm{G}}}}^{(0)}\left(u.v \mid x_2 : \omega, k_1, k_3\right) + \bar{\bar{\bar{\mathrm{G}}}}^{(0)}\left(u, v \mid x_2 : \omega, k_1, -k_3\right)\right] = \frac{1}{2}\left[\bar{\bar{\bar{\mathrm{G}}}}^{(0)}\left(0\mp \quad \right.\right. \quad \left.\left., k_1, k_3\right)\right.$$

$$\left.+\bar{\bar{\bar{\mathrm{G}}}}^{(0)}\left(0\mp \quad \right.\right. \quad \left.\left., k_1, -k_3\right)\right] = \frac{-k_\infty^2 e^{\mp \sqrt{\quad - k_\infty^2}\, x_2}}{(2\pi)^3\sqrt{k_1^2 + k_3^2 - k_\infty^2}} H\left(x_2 y_2\right)\left[1 + O\left(k_\infty^2\right)\right], \text{ for } x_2 \gtrless 0 \tag{5.20}$$

A similar analysis for the antisymmetric component shows that the inner solution $\bar{\bar{\bar{G}}}^{(0)}\left(u, v \mid x_2 : \omega, k_1, k_3\right) - \bar{\bar{\bar{G}}}^{(0)}\left(u, v \mid x_2 : \omega, k_1, -k_3\right)$ turns out to be at least $O\left(k_\infty\right)e^{\mp \sqrt{\quad - k_\infty^2}\, x_2}$ and the antisymmetric contribution to $\bar{\bar{\bar{G}}}^{(0)}\left(u, v \mid x_2 : \omega, k_1, k_3\right)$ can consequently be neglected. It therefore follows from equations (5.6)and (5.7) that the scattered component $\bar{\bar{\bar{G}}}^{(s)}\left(u, v \mid x_1, x_2 : \omega, k_1, k_3\right)$ of the Fourier transformed low frequency Green's function $\bar{\bar{\bar{G}}}\left(u, v \mid x_1, x_2 : \omega, k_1, k_3\right)$ is given by

$$\bar{\bar{\bar{G}}}^{(s)}\left(u, v \mid x_1, x_2 : \omega, k_1, k_3\right) = \bar{\bar{\bar{G}}}_+^{(s)}\left(u, v \mid x_1, x_2 : \omega, k_1, k_3\right) + \bar{\bar{\bar{G}}}_-^{(s)}\left(u, v \mid x_1, x_2 : \omega, k_1, k_3\right)$$

$$= \overline{\overline{\overline{G}}}_{+}^{(s)}\left(u,v\,|\,x_1,x_2:\omega,k_1,k_3\right)+O\left(k_\infty^2\right) \qquad (5.21)$$

Appendix D shows that the Fourier transform of the symmetric component of the scattered component of the Green's function is of the form

$$\overline{\overline{\overline{G}}}_{+}^{(s)}\left(u,v\,|\,x_1,x_2:\omega,k_1,k_3\right)=A_{\gtrless}^{(s)}\left\{1\mp\int_0^u\frac{\left[M(u)k_1/k_\infty-1\right]^2}{c^2(u)}du-\right.$$

$$\left.\sqrt{k_1^2+k_3^2-k_\infty^2}\sum_{n=-\infty}^{\infty}e^{inv}\hat{P}_n^{\gtrless}\left(u:\omega,k_1\right)+O\left(k_1^2+k_3^2-k_\infty^2\right)\right\},\quad \text{for } u\lessgtr 0 \qquad (5.22)$$

6. An application of the general theory -Interaction of a jet and other shear flows with a trailing edge

6.1 Formulation

The scattered component of the Fourier transformed Green's function can usually be found by using the Weiner-Hopf technique (Noble, 1958). We illustrate this by considering the specific case of a three-dimensional jet-like shear flow interacting with an impermeable flat plate that lies as $u=0$, $-\infty<y_1\leq 0$ and suppose for definiteness that the mean velocity, say $U(u)$, vanishes at $u\to 0$ and that the distance between the nozzle exit and the trailing edge is of the same order as the decay scale of the turbulent eddies. The disparate length scales then ensure that the upstream boundary conditions can be imposed in a region that is at a finite distance from the nozzle flow field while still being at an infinite distance upstream of the trailing edge on the scale of the interaction. This region may still be affected by the details of the downstream influence of the nozzle exit flow, such as the level and nature of the disturbances, as well the initial momentum thickness of the wall shear layers. But these effects are now accounted for by specifying the mean velocity profile $U(u)$, the distance $A\left(u,v\middle|\tilde{\imath}\ \tilde{\ }\right.$ and structure of the upstream turbulence spectrum(4.22).

A typical configuration for which the $W\to z$ mapping (A.1) (see figure A.1) applies is shown in figure 3.

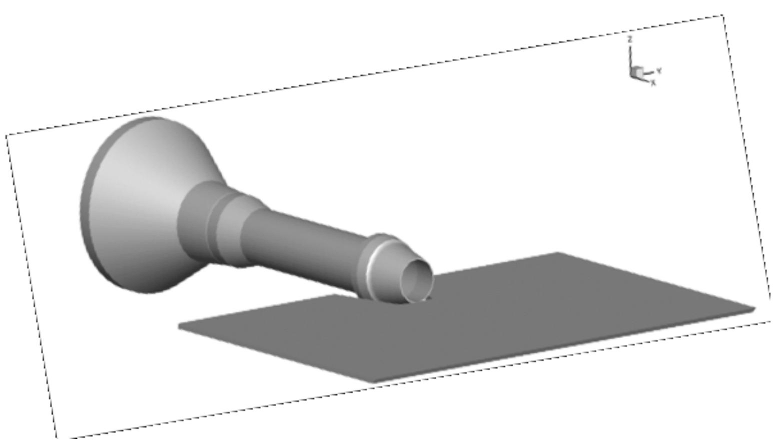

Figure 3. Round jet surface interaction

6.2 The Fourier transformed Green's function

We begin by setting

$$\hat{G}_{\gtrless}\left(u,v\,|\,x_1,x_2:\omega,k_1,k_3,\right)\equiv e^{ik_1x_1}\overline{\overline{\overline{G}}}^{(s)}_{\pm}\left(u,v\,|\,x_1,x_2:\omega,k_1,k_3\right),\ \text{ for }\ u\lessgtr 0, \tag{6.1}$$

where the + sign corresponds to the symmetric case and the – sign to the antisymmetric case alluded to above, and are unrelated to the $\gtrless$ subscript. The functions $\overline{\overline{\overline{G}}}^{(s)}_{\pm}\left(u,v\,|\,x_1,x_2:\omega,k_1,k_3\right)$, for $u\lessgtr 0$, denote specific homogeneous solutions of the spanwise Fourier transform of equation (5.3) that have outgoing wave behavior as $y_2=\pm\infty$, respectively.

The hydrodynamic component $\overline{\overline{\overline{G}}}^{(0)}\left(u,v\,|\,x_1,x_2:\omega,k_1,k_3\right)$ can be identified with the inhomogeneous solution of (5.3)that satisfies the homogeneous boundary condition (5.10) and can, without loss of generality, be required to vanish for $ux_2>0$ so that

$$\overline{\overline{\overline{G}}}^{(0)}\left(u,v\,|\,x_1,x_2:\omega,k_1,k_3\right)=\overline{\overline{\overline{G}}}^{(0)}\left(u,v\,|\,x_2:\omega,k_1\right)=0,\ \text{ for } ux_2>0, \tag{6.2}$$

Applying the boundary condition(2.8) and the jump conditions(2.10) and using (2.9), (3.4) and (6.1) now leads to the following Wiener Hopf problem for $\hat{G}_{\lessgtr}$

$$\int_{-\infty}^{\infty}e^{-ik_1y_1}\hat{G}'_{>}\left(0,v\,|\,x_1,x_2:\omega,k_1,k_3\right)dk_1=0,\quad -\infty<\ y_1<0, \tag{6.3}$$

$$\int_{-\infty}^{\infty}e^{-ik_1y_1}\left[\hat{G}'_{>}\left(0,v\,|\,x_1,x_2:\omega,k_1,k_3\right)-\hat{G}'_{<}\left(0,v\,|\,x_1,x_2:\omega,k_1,k_3\right)\right]dk_1=0,\quad -\infty<\ y_1<\infty, \tag{6.4}$$

and

$$\int_{-\infty}^{\infty}e^{-ik_1y_1}\left[\hat{G}_{>}\left(0,v\,|\,x_1,x_2:\omega,k_1,k_3\right)-\hat{G}_{<}\left(0,v\,|\,x_1,x_2:\omega,k_1,k_3\right)\right]dk_1$$

$$+\frac{1}{2}\int_{-\infty}^{\infty}e^{ik_1(x_1-y_1)}\Delta\left[\overline{\overline{\overline{G}}}^{(0)}\left(0,v\,|\,x_2:\omega,k_1,k_3\right)\pm\overline{\overline{\overline{G}}}^{(0)}\left(0,v\,|\,x_2:\omega,k_1,-k_3\right)\right]dk_1=0,\quad 0<y_1<\infty, \tag{6.5}$$

with the notation $\Delta[\square]$ being defined below (2.10)and $\hat{G}'_{\lessgtr}\left(0,v\middle|x_1,x_2:\omega,k_1,k_3\right)$

$\equiv\partial\hat{G}_{\lessgtr}\left(u,v\middle|x_1,x_2:\omega,k_1,k_3\right)/\partial u\Big|_{u=0}$.

6.3 Low frequency limit

For reasons given above, we now consider the low frequency limit. It then follows from (5.22) and(6.1) that (6.4)will be satisfied if

$$A_{>}^{(s)}\left(x_1,x_2;k_1,k_3,k_\infty\right)=-A_{<}^{(s)}\left(x_1,x_2;k_1,k_3,k_\infty\right) \tag{6.6}$$

and

$$a_{>}=a_{<}. \tag{6.7}$$

while inserting (D.3) into (5.22), closing the integration contour in the upper half k_1 -plane and using Cauchy's theorem shows that (6.3) will be satisfied if (see(6.1))

$$2e^{ik_1x_1}A_{>}^{(s)}\left(x_1,x_2;k_1,k_3,k_\infty\right)/\Gamma_0\left(k_1,k_3,k_\infty\right)=H_+\left(x_1,x_2;k_1,k_3,k_\infty\right) \tag{6.8}$$

and

$$e^{ik_1x_1}A_{>}^{(s)}\left(x_1,x_2;k_1,k_3,k_\infty\right)a_{>}=\tilde{I}_{+}\left(x_1,x_2;k_1,k_3,k_\infty\right), \tag{6.9}$$

where $H_+\left(x_1,x_2;k_1,k_3,k_\infty\right)$, $\tilde{I}_{+}\left(x_1,x_2;k_1,k_3,k_\infty\right)$ denote analytic functions in the upper half k_1 -plane and

$$\Gamma_0\equiv-\frac{2}{\sqrt{k_1^2+k_3^2-k_\infty^2}} \tag{6.10}$$

Then since (Lighthill, 1964)

$$\lim_{u\to 0}\sum_{n=-\infty}^{\infty}e^{inv\pm|n|u}=\sum_{n=-\infty}^{\infty}e^{inv}=2\pi\delta\left(v\right) \tag{6.11}$$

inserting (6.6), (6.8) and(5.22) into(6.5) leads to the following standard Weiner Hopf problem

$$\int_{-\infty}^{\infty}e^{-ik_1y_1}H_+\Gamma_0\left[1+O\left(k_1^2+k_3^2-k_\infty^2\right)\right]dk_1=-\frac{1}{2}\int_{-\infty}^{\infty}e^{ik_1(x_1-y_1)}\Delta\Big[\overline{\overline{\mathrm{G}}}^{(0)}\left(0,v\,|\,x_2:\omega,k_1,k_3\right)$$

$$\pm\overline{\overline{\mathrm{G}}}^{(0)}\left(0,v\,|\,x_2:\omega,k_1,-k_3\right)\Big]dk_1,\ \text{for}\ y_1>0\ \ \text{and}\ \ 0<|v|\le\pi \tag{6.12}$$

which is formally the same as the one given by equations (B2) and (B3) of Goldstein et al (2013a) and it therefore follows from equations (B9) and (B12) of that reference and equation (5.20) of the present paper that

$$H_+\left(x_1,x_2:k_\infty,k_1,k_3\right)\equiv$$

$$-\frac{1}{4\pi i}\int_{-\infty}^{\infty}e^{i\tilde{k}_1x_1}\frac{\kappa_-\left(\tilde{k}_1,k_3,v\right)\Big[\overline{\overline{\mathrm{G}}}^{(0)}\left(0,v\,|\,x_2:\omega,\tilde{k}_1,k_3\right)-\overline{\overline{\mathrm{G}}}^{(0)}\left(0,v\,|\,x_2:\omega,\tilde{k}_1,-k_3\right)\Big]}{\kappa_+\left(k_1,k_3,0\right)\left(\tilde{k}_1-k_1\right)}d\tilde{k}_1,$$

$$= \frac{k_\infty^2 \operatorname{sgn} x_2}{(2\pi)^4 i} \int_{-\infty}^{\infty} e^{i\tilde{k}_1 x_1} \frac{\kappa_-\left(\tilde{k}_1, k_3, 0\right) e^{-\sqrt{\tilde{k}_1^2 + k_3^2 - k_\infty^2}\, x_2}}{\left(\tilde{k}_1 - k_1\right)\kappa_+\left(k_1, k_3, 0\right)\sqrt{\tilde{k}_1^2 + k_3^2 - k_\infty^2}} d\tilde{k}_1, \quad \text{for } x_2 \gtrless 0 \tag{6.13}$$

where the integration contour must be deformed to lie below the poles of the integrand in order to satisfy causality, $\kappa_\pm\left(k_1, k_3, v\right)$ denote bounded analytic functions in the upper/lower half k_1 planes that satisfy the factorization condition

$$\kappa_+\left(k_1, k_3, v\right)/\kappa_-\left(k_1, k_3, v\right) = \Gamma_0\left(k_\infty, k_1, k_3\right) \equiv -\frac{2}{\sqrt{k_1^2 + k_3^2 - k_\infty^2}} \tag{6.14}$$

on the real k_1 −axis with the $\tilde{k}_1$ -integration contour in (6.13) being deformed to pass below the pole at $\omega / U(u) = k_1$. But this integral can be interpreted as a Cauchy principal value when evaluating the far-field behavior of(5.6), since the contribution from that pole produces a term that behaves like $\exp\left[i\omega x_1 / U(u)\right]$, which produces the non- radiating hydrodynamic disturbance $\overline{p}^{(0)}\left(\boldsymbol{x} : \omega, T\right)$ at subsonic speeds.

The $O\left(k_1^2 + k_3^2 - k_\infty^2\right)$ error term in (6.12) is important because it shows that the error on the left hand side is consistent with the right hand side error implied by(5.20).

Causality considerations (Briggs, 1964 and Bers, 1975) then require that

$$\kappa_-\left(k_1, k_3, 0\right) = \sqrt{k_1 - \sqrt{k_\infty^2 - k_3^2}} + .., \kappa_+\left(k_1, k_3, 0\right) = \frac{-2}{\sqrt{k_1 + \sqrt{k_\infty^2 - k_3^2}}} + .., \tag{6.15}$$

where the branch cuts are chosen so that $\arg\sqrt{k_1^2 + k_3^2 - k_\infty^2} = -(\pi/2) H\left(k_1^2 + k_3^2 - k_\infty^2\right)$.

Goldstein et al (2017) found that the lowest-order approximation to the low-frequency Green’s function for the planar jet is independent of the mean flow and is therefore equal to low frequency limit of the zero-mean-flow Green’s function. The lowest order approximation to the Fourier transformed Green’s function (5.22) must also reduce to the zero-mean-flow Green’s function, and therefore to the low frequency Green’s function obtained by Goldstein et al (2013a), when the mean flow goes to zero. But this can only occur if $a_{\gtrless} = o\left(k_\infty\right)$ and equations(5.6), (5.7), (5.22) and (6.8)therefore show that the lowest order approximation to Fourier transform of the scattered component of the Green’s function $\overline{\overline{G}}^{(s)} = \overline{\overline{G}}_+^{(s)} + \overline{\overline{G}}_-^{(s)} \approx \overline{\overline{G}}_+^{(s)}$ is given by

$$\overline{\overline{G}}^{(s)}\left(u, v \,|\, \boldsymbol{x} : \omega, k_1\right) = e^{-ik_1 x_1} \int_{-\infty}^{\infty} e^{ik_3 x_3} \left(\Gamma_0 / 2\right) H_+\left(x_1, x_2 : k_\infty, k_1, k_3\right) dk_3, \ \text{for } u < 0 \tag{6.16}$$

As in Goldstein et al (2017) the Green’s function (6.13) ,(6.15) and (6.16) is independent of the mean flow and the wall normal coordinate and is therefore the same as the low-frequency limit of the zero mean flow Green’s function which can be calculated by well know classical methods. We expect this finding to be quite universal and to apply to all low frequency transversely sheared RDT problems. The

present Green's function also becomes independent of the spanwise coordinate y_3 in the source region which is now confined to the spanwise location where $y_3 = O(1)$.

6.4 The pressure spectrum

Inserting (6.13) into(6.16), using the result into (3.1) and(2.25), changing the integration variables from y_2, y_3 to u, v and noting that the Green's function is independent of v shows that

$$\bar{p}^{(s)}(\boldsymbol{x},\omega) = \operatorname{sgn} x_2 \int_{-\infty}^{0} \boldsymbol{\mathcal{R}}(u,\boldsymbol{x},\omega)\tilde{\Omega}(\cdot,\cdot,\cdot)\,du, \tag{6.17}$$

where we have put

$$\boldsymbol{\mathcal{R}}(u,\boldsymbol{x},\omega) \equiv \frac{k_\infty^2}{4\pi i}\int_{-\infty}^{\infty}\int_{-\infty}^{\infty} e^{i\Psi}\,\frac{\sqrt{\tilde{k}_1 - \sqrt{k_\infty^2 - k_3^2}}\;\tilde{\cdot}}{\sqrt{\omega/U(u) - \sqrt{k_\infty^2 - k_3^2}}\,\sqrt{\tilde{k}_1 - k_\infty + k_3}\,\left[\tilde{k}_1 - \omega/U(u)\right]}\,dk_3, \tag{6.18}$$

$$\tilde{\Omega}(\cdot,\cdot,\cdot) \quad \frac{1}{2\pi}\left[\int_{-\pi}^{\pi} \bar{\Omega}(u,v,\omega)\left|\frac{dW}{dz}\right|^{-2} dv\right] \tag{6.19}$$

and

$$\Psi \equiv k_3 x_3 + \tilde{k}_1 \cdot_1 \mp \sqrt{\tilde{\quad} \cdot_3 \cdot_2}. \tag{6.20}$$

6.5 Far field behavior of the low frequency acoustic spectrum

Equation (6.20) can be written as

$$\Psi = \vartheta|\boldsymbol{x}| \tag{6.21}$$

where

$$\vartheta \equiv k_1\cos\theta + i\sqrt{k_1^2 + k_3^2 - k_\infty^2}\,\sin\theta\sin\psi + k_3\sin\theta\cos\psi, \tag{6.22}$$

$|\boldsymbol{x}|^2 \equiv x_1^2 + x_2^2 + x_3^2$ and we have introduced the polar coordinate system $\boldsymbol{x} = |\boldsymbol{x}|\{\cos\theta, \sin\theta\sin\psi, \sin\theta\cos\psi\}$ with the polar angle θ being measured from the downstream direction.

The integrals in equation(6.18) can be evaluated by sequentially applying the method of stationary phase to obtain

$$\boldsymbol{\mathcal{R}}(u,\boldsymbol{x},\omega) \equiv \frac{k_3^{(s)}}{|\boldsymbol{x}|}e^{i|\bar{\boldsymbol{x}}|k_\infty}\,\frac{\sqrt{k_1^{(s)} - \sqrt{k_\infty^2 - \left(k_3^{(s)}\right)^2}}}{\sqrt{\omega/U(u) - \sqrt{k_\infty^2 - \left(k_3^{(s)}\right)^2}}\,\sqrt{\left(k_1^{(s)}\right)^2 - k_\infty^2 + \left(k_3^{(s)}\right)^2}\left[k_1^{(s)} - \omega/U(u)\right]}$$

$$= \frac{k_\infty e^{i|\boldsymbol{x}|k_\infty} M^{3/2}\sqrt{\beta - \cos\theta}}{2|\boldsymbol{x}|\sqrt{1-\beta M(u)}\left[1 - M(u)\cos\theta\right]} \tag{6.23}$$

as $|\bar{\boldsymbol{x}}|, x_2 \to \pm\infty$, where

$$k_3^{(s)} = k_\infty \sin\theta\cos\psi, \quad k_1^{(s)} = k_\infty \cos\theta \tag{6.24}$$

denote the stationary phase points, the local Mach number $M(u)$ is given by (5.13)and

$$\beta \equiv \sqrt{1-\sin^2\theta\cos^2\psi}. \tag{6.25}$$

Using equations (6.17) along with (6.23),(4.21),(6.19) and (6.21) in (4.19) therefore shows that the far-field acoustic spectrum is given in terms of the source spectrum by

$$I_\omega(\boldsymbol{x}) = \left(\frac{k_\infty}{4\pi|\bar{\boldsymbol{x}}|}\right)^2 \int_{-\infty}^{0}\int_{-\infty}^{0} \frac{(\beta-\cos\theta)\left[M(u)M(\tilde{u} \; \ldots\right.}{\sqrt{\left[1-\beta M(\tilde{u} \; \ldots \cos\theta\right]}} \tag{6.26}$$

where

$$\bar{S}(u,\tilde{u} \; \ldots \int_{-\pi}^{\pi}\int_{-\pi}^{\pi} \ldots \left|\frac{dz}{dW}\right|^2 \left|\frac{d\tilde{z}}{d\tilde{W}}\right| \ldots \tag{6.27}$$

and the source spectrum S is given by (4.21). These results are independent of the actual form of the conformal mapping $z \to W$ and are therefore expected to apply to any sufficiently localized flow configuration (such as the multiple jet configuration shown in figure 1) that can be conformally mapped into a strip similar to the one shown in figure A.1. In fact, it can probably be extended to zero-surface velocity flows with arbitrary cross section by replacing $|dz/dW|^2$ with the Jacobian $\partial(y_2, y_3)/\partial(u,v)$ of the transformation of the rectangular y_2, y_3 coordinate system into any orthogonal coordinate system for which $U(\boldsymbol{y}_T) = U(u)$.

6.6 Extension to higher frequencies

The practical utility of the low frequency solution(6.26) and (6.27) can be increased by extending it to higher frequencies. To this end we note that the Fourier transform of the $O(1)$ frequency zero mean flow Green's function only differs from its low frequency limit by a factor of $\exp\left(-\sqrt{k_\infty^2 - k_1^2 - k_3^2}\,|y_2|\right)$ (as can easily be seen by replacing the outgoing wave solution $P_>(y_2|x_1, x_2 : \omega, k_1, k_3)$ in the Wiener-Hopf solution (6.13), (6.15)and (6.16) with the zero mean flow outgoing wave solution $\exp\left(-\sqrt{k_\infty^2 - k_1^2 - k_3^2}\,y_2\right)$). We therefore expect that (6.26) will perform better at higher frequencies if we replace (6.27)with

$$\bar{S}(u,\tilde{u} \; \ldots \int_{-\pi}^{\pi}\int_{-\pi}^{\pi} \ldots \left|\frac{dz}{dW}\right|^2 \left|\frac{d\tilde{z}}{d\tilde{W}}\right| \ldots \tag{6.28}$$

where

$$Q(u,v) \equiv e^{-k_\infty\sqrt{1/M^2(u)-\beta^2}\,y_2(u,v)} \tag{6.29}$$

and

$$y_2(u,v)=\frac{1}{2}\frac{1-e^{2u}}{1-2e^{u}\cos v+e^{2u}} \tag{6.30}$$

7. Numerical results

Measurements of the noise generated by the interaction of a circular jet with the trailing edge of a flat-plate were carried out by Brown (2013, 2015a, b) in the Small Hot Jet Acoustic Rig (SHJAR) at the Aero-Acoustic Propulsion Laboratory (AAPL) at NASA Glenn Research Center (Bridges and Brown, 2005; Brown and Bridges, 2006). The experimental configuration along with the relevant geometric parameters are shown in figure 4. Our interest here in comparing the present analysis with these measurements and it seems reasonable to assume that the mean surface velocity is zero and this setup, so that , as indicated above, the model problem considered in Sections 7and 8 can be used to represent this interaction. The analysis is basically inviscid but accounts for viscous effects by imposing a Kutta (or minimum singularity) condition at the trailing edge (Goldstein et al,2013). Similar but more complicated analyses would be required to deal with the case where the mean surface velocity is non-zero.

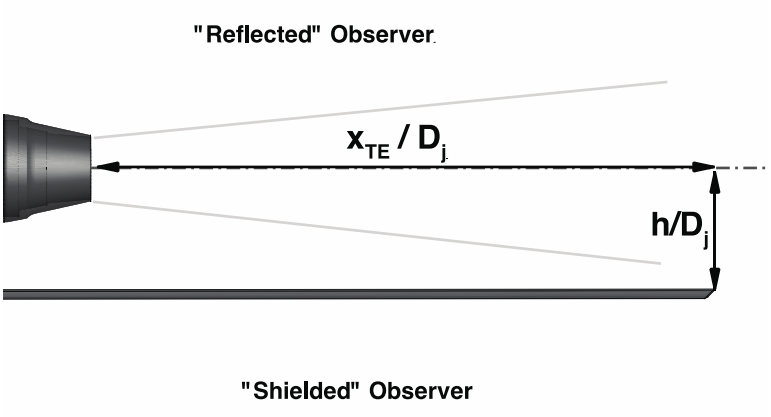

Figure 4 – Experimental configuration. From Brown (2013), used with permission'

It is also reasonable to suppose that the constant velocity surfaces can be represented by the conformal mapping (A.1) for a single jet configuration of this type. And we assume in the calculations that the mean density ρ is constant and the mean velocity profile $U(y_2,y_3)$ can be represented by a symmetric function of the form

$$U(u)=U_d\left(1-e^{-\kappa u^2-\kappa_1 u^4}\right), \tag{7.1}$$

where κ and κ_1 are constants. And since the amplitude factor $A(u,v|\tilde{\imath}\ \tilde{}$ in (4.22) must vanish at the jet boundaries and is determined by strength of the turbulence at the source location, we expect it to be proportional to the turbulence intensity at u,v which is roughly proportional to the mean velocity gradient at that point. We therefore set

$$A\left(u,v\right|\tilde{\imath} \ldots \quad \text{[illegible]} \tag{7.2}$$

where A_0 is a positive constant. Jet flow measurements suggest that is also reasonable to choose the arbitrary function $f\left(\eta_2 / l_2, \eta_3 / l_3\right)$ in the velocity correlation model (5.7) to be $f\left(\eta_2 / l_2, \eta_3 / l_3\right) = \left|\eta_2 / l_2 + \eta_3 / l_3\right|$, where, l_2 and l_3 dente constant the length scales.
Brown (2013, 2015a, b) considered many combinations of the axial and radial locations of the plate trailing edge relative to the nozzle exit and a wide range of jet flow conditions. Their nozzle diameter D_j was approximately equal to two inches and noise measurements were made on both the shielded and reflected observer locations (see Figure 4). We decided to use the unheated jet results for the three jet exit acoustic Mach numbers $M_a = 0.5, 0.7, 0.9$ and selected the configuration where the plate was located at one nozzle diameter from the jet centerline and the trailing edge was located six diameters downstream of the nozzle exit as an initial test case for the theory, since this configuration resulted in some of the highest levels of trailing-edge noise observed in the experiments. The scale factor h , which was taken to be the distance between the nozzle centerline and the plate, was equal to the nozzle diameter D_j in this case.

The numerical results were computed from the formula (6.26)for the acoustic spectrum, with $\overline{S}$ determined from (8.55) – (8.57) and (A.5), and S given by the source model (5.8). The u and $\tilde{\imath}$ integrations were carried out by using Simpsons rule, truncating the lower limits at 'large' but finite negative values of these quantities and using the fact that the integrands vanish at $u, \tilde{\imath}$. The lower limits of the integrations were set equal to -2.0 in the calculations shown in the figures. The u -integrals were computed with 100 mesh points while 128 points were used to evaluate the v -integrals, which were also computed from Simpson's rule. Numerical testing was carried out to ensure that these integration parameter values were sufficient to produce results that differed by less than hundredths of a dB.

The mean velocity parameters κ and κ_1 were both set equal to 0.5 in the computations and the resulting profile shape is shown in figure 5.

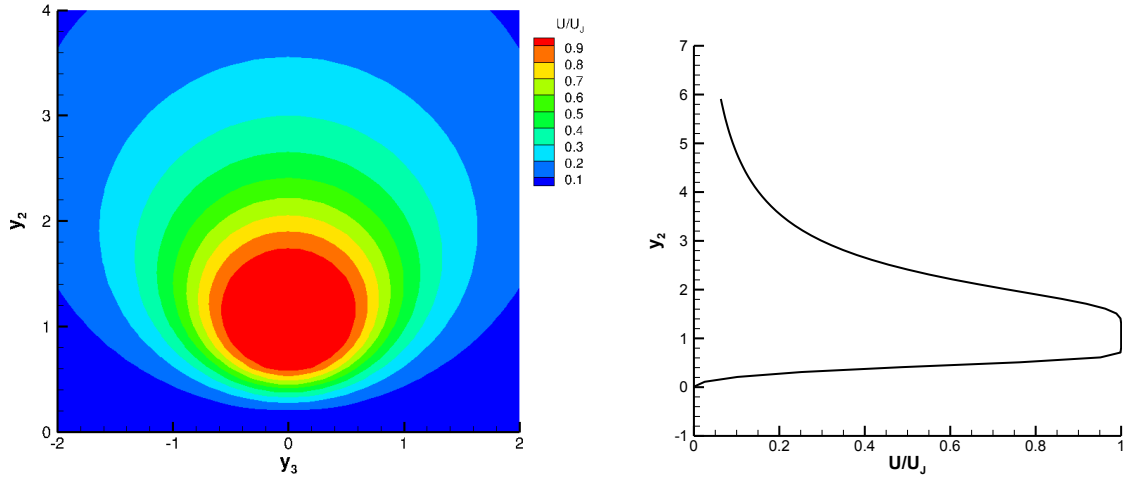

a) b)

Figure 5. Normalized mean velocity profiles calculated from (7.1) with $\kappa = \kappa_1 = 0.5$, a) altitude plot, b) profile shape at $y_3 = 0$.

Figure 6 is contour plot of the amplitude function(7.2) used in the computation. It clearly shows that the turbulence level vanishes at the edge of the jet and that its maximum intensity roughly coincides with the region of maximum shear.

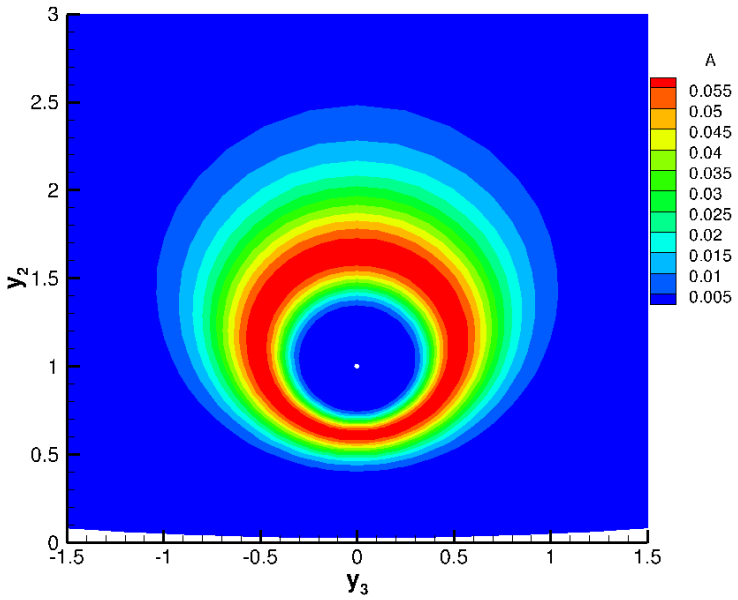

Figure 6 Contour plot of amplitude function (7.2) with $A_0 = 0.035$

Figures 7 through 9 are quantitative comparisons of the measurements of Brown (2013, 2015a, b) with theoretical predictions obtained from composite RDT solution(6.26),(6.28) and (6.29). Results for the power spectral density of the far-field pressure fluctuation vs. Strouhal number, St $= f\,h/U_J$, in dB scale $PSD = 10\log(4\pi I_\omega U_J / h\,p_{ref}^2)$ (referenced to $p_{ref} = 20\mu pa$) are shown at several polar angles measured from the downstream jet axis. The experimental trailing-edge noise was educed by subtracting the noise measured in the corresponding free jet (i.e., in the absence of a plate) from the total measured noise. The remaining parameters used in the predictions shown in the figures are $\tau_0 = 2.8, l_2 = 2.13$ and $l_3 = 0.75$.

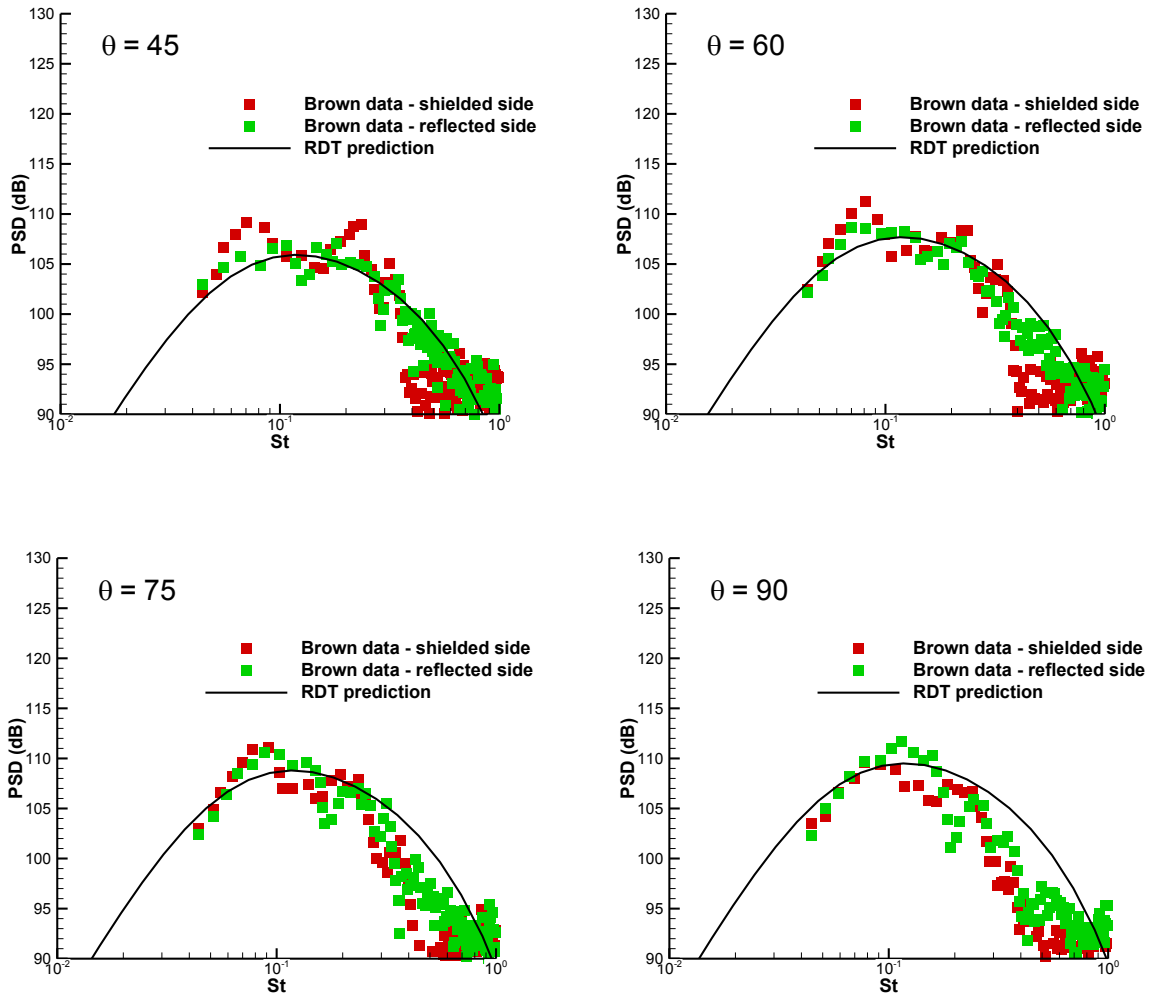

Figure 7 – Comparisons of noise predictions using the composite RDT solution (8.53) and (8.55) – (8.57) (solid lines) with experimental data. Ma = 0.5.

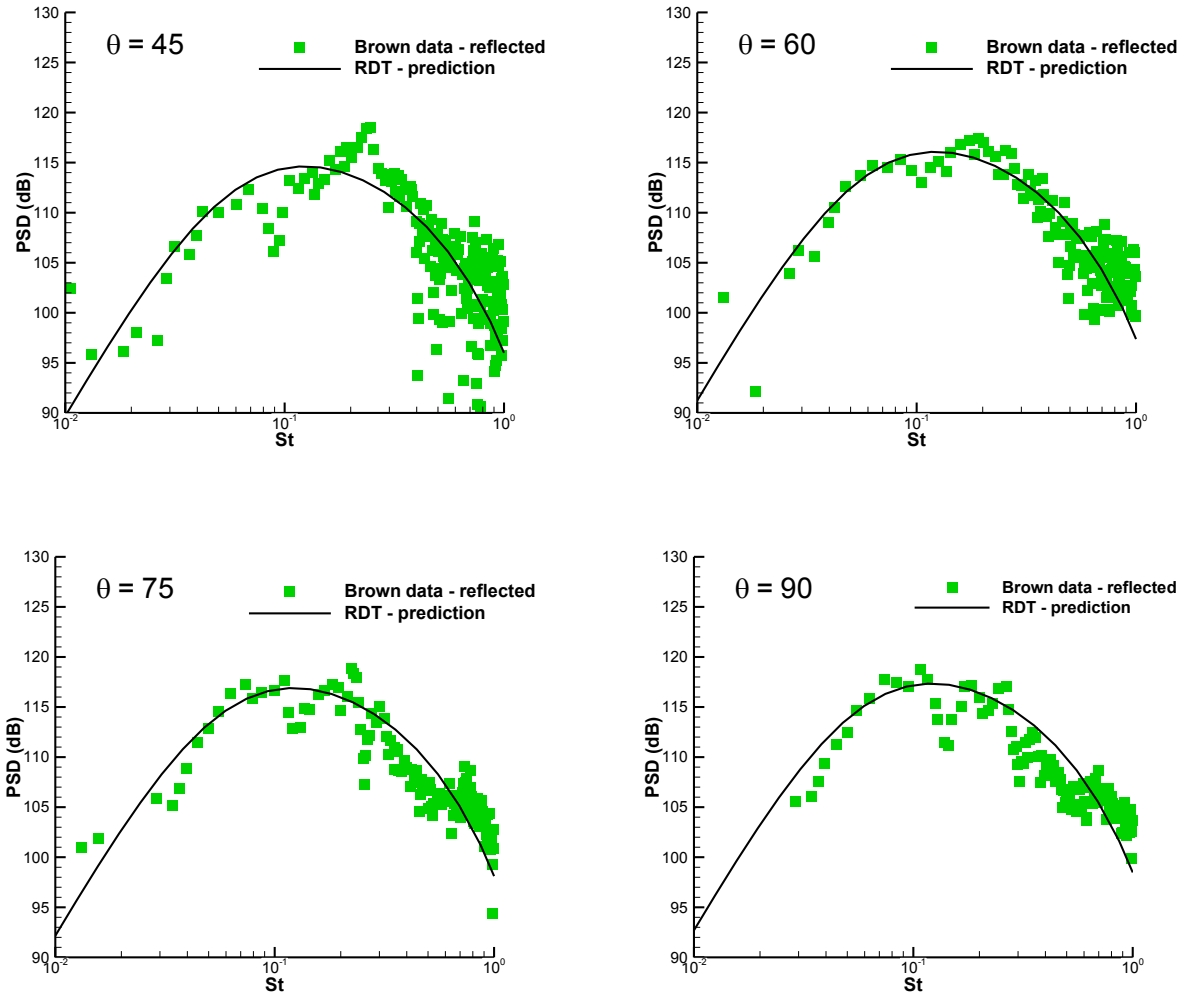

Figure 8- Comparisons of noise predictions using the composite RDT solution (8.53) and (8.55) – (8.57) with experimental data. Ma = 0.7.

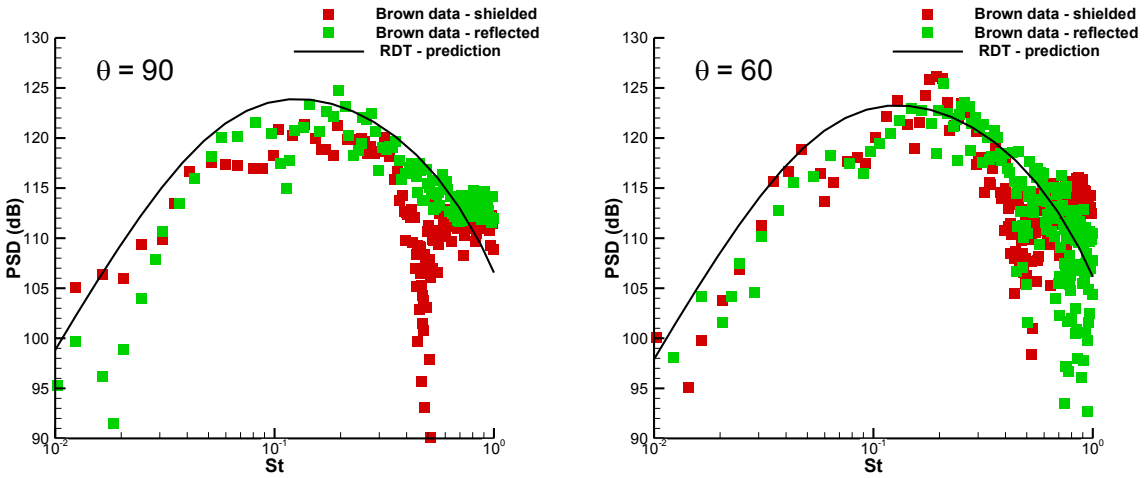

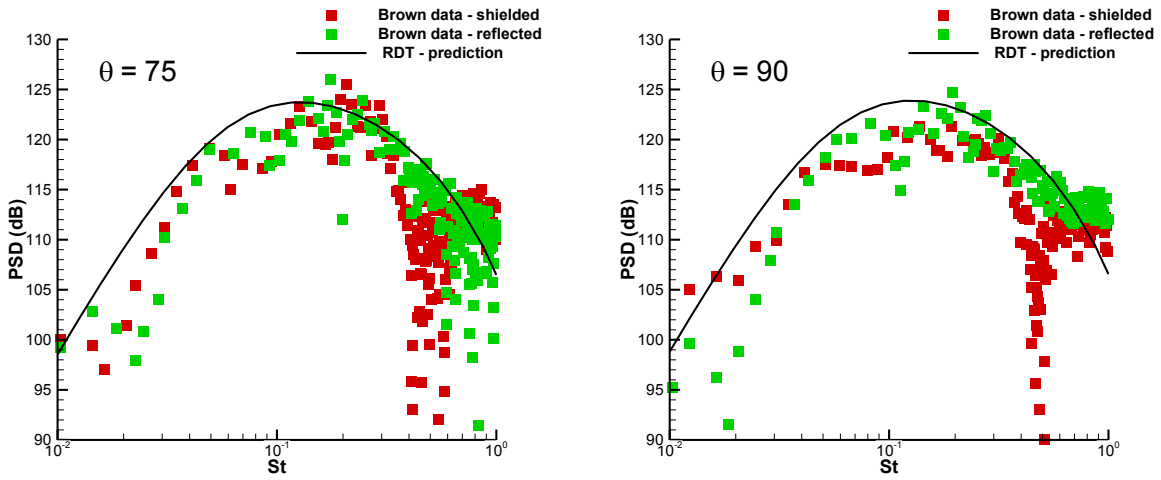

Figure 9 - Comparisons of noise predictions using the composite RDT solution (8.53) and (8.55) – (8.57) (solid lines)with experimental data. Ma = 0.9.

These comparisons show that the theoretical predictions are in reasonable agreement with the data—especially at frequencies near and below the spectral peaks —and that the experimental results are well captured at all Mach numbers considered. The zero-mean flow-based high-frequency correction reduces the spectral levels at frequencies beyond the peak and causes the slope of the roll-off to more closely follow the data. But the accuracy of the predictions is relatively unimportant in this region, since the edge noise is well below the jet noise at these frequencies. The agreement seems to be worse at the highest Mach number (Ma = 0.9) shown in the figures, but there is significant scatter in the data for this case, which may be due to the difficulty in extracting the edge noise at this higher Mach number, where the jet noise starts to become comparable to the trailing-edge noise -- even at the lower frequencies.

The accuracy of the predictions in Figures 7-9 at frequencies near and below the spectral peaks is comparable to that obtained by Goldstein et al (2017) for the case of a planar jet. Differences can perhaps be attributed to uncertainty in the source parameter values and more scatter in the extracted experimental edge-noise data in the present round jet case.

The numerical results in Figures 7-9, along with our previous results for a planar jet (Goldstein et al 2017), show that the RDT can be used to predict the noise generated by the interaction of a turbulent jet with the trailing-edge of a flat plate. This flow configuration models the situation encountered when a jet engine is tightly integrated into an airframe (as illustrated in Figure 1) and the relatively simple formula for the acoustic spectrum allows a quick assessment of the additional noise generated by the–surface interaction.

8. Concluding Remarks

This paper is based on the formal solutions (2.4) and (2.11)-(2.14) to the linearized Euler equations (2.2) and (2.3) for transversely sheared mean flows which, like the classical Kovasznay (1953) result for the unsteady motion on uniform flows, involve two arbitrary convected quantities $\vartheta\left(\tau - y_1 / U, \boldsymbol{y}_T\right)$ and

[illegible] $U,\boldsymbol{y}_T\big)$, that can be associated with the hydrodynamic component of the flow and can, therefore, be used to specify upstream boundary (i.e., initial) conditions for RDT problems that involve the interaction of turbulence with solid surfaces. The results were applied to the specific case of a round jet interacting with the trailing edge of a flat plate and an explicit low frequency solution was obtained. The low-frequency Green's function that appears in this result is independent of the mean flow when evaluated in terms of the streamwise wave number k_1 just as it was for the two dimensional mean flow considered in Goldstein et al (2017). This means that these low frequency Green's functions are the same as the low frequency limit of the zero-mean flow Green's function which can usually be found by using well known standard techniques (Noble, 1958). This finding appears to be quite generic and probably applies to many transversely sheared RDT problems. The final formula (6.26) turns out to be independent of the actual form of the conformal mapping $z \to W$ and can probably be extended to any sufficiently localized flow (such as the multiple jet configuration shown in figure 1) by replacing $\left|dz/dW\right|^2$ with the Jacobian $\partial\left(y_2, y_3\right)/\partial\left(u, v\right)$ of an appropriate mapping .

Appendix A. Conformal mapping

The specific realization

$$W = \ln\frac{z-i}{z+i} \tag{A.1}$$

of the transform(5.1),(5.2) that maps the strip $-\pi \le v \le \pi$, $-\infty < u < \infty$ into the entire $z-$ plane can be inverted to obtain

$$z = i\frac{1+e^W}{1-e^W} = -i\coth\frac{W}{2}. \tag{A.2}$$

And it follows from Abramowitz and Stegun (1964, p85, # 4.5.67) that

$$z \to -i\left(\frac{2}{W} + \frac{W}{3} - \frac{W^3}{360} + O\left(W^5\right)\right) + \ldots \text{ as W} \to 0, \tag{A.3}$$

$$\frac{dz}{dW} = \frac{i}{2\sinh^2\left(W/2\right)}, \tag{A.4}$$

$$\left|\frac{dz}{dW}\right|^2 = \frac{4}{\left(e^{-u} - 2\cos v + e^{u}\right)^2} \tag{A.5}$$

and therefore that

$$iv = \ln\frac{y_3 - i}{y_3 + i} = -i2\tan^{-1}\left(1/y_3\right) \tag{A.6}$$

when $u = 0$,which shows that $v \to 0$ as $y_3 \to -\infty$ and $v \to \mp$ as $y_3 \to 0\pm$ on the plate surface. Equation(A.1) implies that

$$W \to -2i/z = -2iz^*/y_T^2, \text{ as } \left|z\right| \to \infty \tag{A.7}$$

and

$$u/|W|^2 \to -y_2/2 \quad v/|W|^2 \to -y_3/2 \quad \text{as } |W| \to 0 \tag{A.8}$$

which shows that

$$u \to 0, v \text{ fixed implies } \quad y_2 \to 0 \quad y_3 \text{ fixed} \tag{A.9}$$

and

$$v = O(1) \text{ implies } \; y_3 = (1) \tag{A.10}$$

where

$$y_T \equiv |z|, \;\; y_3 = y_T \cos\psi, \; y_2 = y_T \sin\psi \tag{A.11}$$

This behavior is consistent with the contour plots shown in figures A1 and A2.

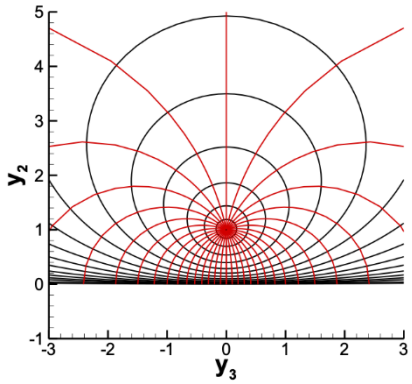

Figure A.1. Level surfaces for the Mapping (A.1)

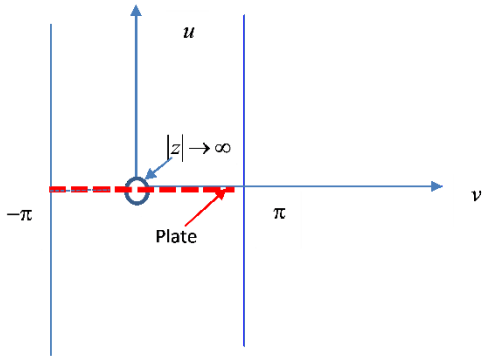

Figure A.2. W-plane for the Mapping (A.1)

Appendix B. Modelling of physically realizable source spectra

The cross correlation

$$\Lambda(\boldsymbol{y}_T,\tilde{\quad}$$

$$=\left\langle \boldsymbol{\mathcal{U}}_\perp(\tau,\boldsymbol{y}_T)\boldsymbol{\mathcal{U}}_\perp\left(\tau+\tilde{\quad}\right.\right. \tag{B.1}$$

of $\boldsymbol{\mathcal{U}}_\perp\left(\tau-y_1/U\left(\boldsymbol{y}_T\right),\boldsymbol{y}_T\right)$ will exist and be independent of τ when $\boldsymbol{\mathcal{U}}_\perp$ is a stationary function of τ and hence also of $\tau-y_1/U\left(\boldsymbol{y}_T\right)$ (Wiener, 1938). It therefore follows that

$$(2\pi)\lim_{T\to\infty}\frac{\bar{\boldsymbol{\mathcal{U}}}_\perp(\boldsymbol{y}_T;\omega,T)\left[\bar{\boldsymbol{\mathcal{U}}}_\perp(\tilde{\quad}\right.}{2T}$$

$$=\frac{1}{2\pi}\int_{-\infty}^{\infty}\exp i\omega\left(\tilde{\quad}\right. \tag{B.2}$$

so that the cross correlation $\Lambda(\boldsymbol{y}_T,\tilde{\quad}$ of the upstream normal velocity derivative fluctuation needs to be specified before the source spectrum (4.21)and therefore pressure spectrum (4.19) can actually be calculated. We are unaware of any actual measurements of this quantity, but it is well known the transverse velocity correlation $\left\langle v_\perp'(\boldsymbol{y},\tau)v_\perp'(\tilde{\quad}\right.$, which has been extensively measured, can be well represented by the exponential form

$$\frac{\left\langle v_\perp'(\boldsymbol{y},\tau)v_\perp'(\tilde{\quad}\right.}{U(\boldsymbol{y}_T)U(y_2,\tilde{\quad}}=A(\boldsymbol{y}_T)\exp-\sqrt{\left\{\tilde{\quad}\right.} \tag{B.3}$$

where l_3 is a constant and U_c denotes an empirically determined constant convection velocity. This is consistent with Taylor's hypothesis (Taylor, 1938) which assumes that the changes in $v_\perp'$ at a fixed point are due to an unchanging pattern of turbulent motion over that point and can be formulated as $v'(y_1,\tau)=v'(y_1-U_c\tilde{\tau}\ \tau\quad\tilde{\tau}$ (Townsend, 1976). Dennis and Nickels (2008) show that the optimal approximation is obtained when U_c is set equal to the local mean velocity $U(\boldsymbol{y})$ (which is equal to $U(\boldsymbol{y}_T)$ for transversely sheared mean flows). But Taylor's hypothesis is an approximation which, as shown by Lin (1953) is only valid when the turbulence level is low, viscous effects are negligible and the mean shear is small. The first two conditions are also required for the validity of Rapid Distortion Theory but the third is definitely not.

The important point is that (B.3) is consistent with the requirements of transversely sheared mean flow RDT when U_c is set equal to $U(y_2)$. But this consistency also requires (see equation(B.1)) that the fully three-dimensional correlation $\left\langle v_\perp'(\boldsymbol{y},t)v_\perp'(\tilde{\quad}\right.$ be represented by the exponential form $A(\boldsymbol{y}_T,\tilde{\quad}\ \sqrt{\left[f(\eta_2/l_2,\eta_3/l_3)\right]^2+\left\{\tilde{\quad}\right.}$,

where τ_0,l_2,l_3 are constants,

$$\eta_2 \equiv u - i\tilde{\quad}\quad\tilde{\quad} \tag{B.4}$$

and $A\left(\boldsymbol{y}_T,\tilde{\quad}\quad/l_2,\eta_3/l_3\right)$ are, yet, unspecified functions of the indicated arguments, rather than by the commonly used form $A(\boldsymbol{y}_T)\exp-\sqrt{\left[f\left(\eta_2/l_2,\eta_3/l_3\right)\right]^2+\left\{\tilde{\quad}\quad\tilde{\quad}\quad c\right]\right\}^2/\tau_0^2}$ - a result that would certainly be worth checking experimentally.

It is therefore seems appropriate to represent $\Lambda\left(\boldsymbol{y}_T,\tilde{\quad}\quad\tilde{\quad}\right.$ $\lim_{y_1\to\quad}\left(y_1\tilde{\quad}\quad\tilde{\quad}\quad\tilde{\quad}\right)=\lim_{y_1\to\quad}\left(y_1\tilde{\quad}\quad\tilde{\quad}\quad\tilde{\quad}\right)$ by $\Lambda\left(\boldsymbol{y}_T,\tilde{\quad}\quad\tilde{\quad}\quad\tilde{\quad}\quad\tilde{\quad}\quad\tilde{\quad}\right)$

$$\exp-\sqrt{\left[f\left(\eta_2/l_2,\eta_3/l_3\right)\right]^2+\left\{\tilde{\quad}\quad\tilde{\quad}\quad\tilde{\quad}\quad\tilde{\quad}\quad u\right)\right]\right\}^2/\tau_0^2} \tag{B.5}$$

where the amplitude $A\left(\boldsymbol{y}_T,\tilde{\quad}\quad\right.$ is expected to vanish as $\boldsymbol{y}_T,\tilde{\quad}\quad$.

And since ρc^2 is constant in transversely sheared flows, inserting this into (B.2) inserting the result into (4.21)and using equation (27) of Leib & Goldstein (2011) shows that (4.22) provides an appropriate model for the source function S (Campbell and Foster, 1948)

Appendix C. The gust component of the low frequency Green's function

The spanwise Fourier transform

$$\tilde{C}\quad\left(\quad\quad:\omega,k_1,k_3\right)\equiv\frac{1}{2\pi}\int_{-\infty}^{\infty}e^{i(y_3-x_3)k_3}\bar{\bar{G}}^{(0)}\left(\boldsymbol{y}_T\,|\,\boldsymbol{x}_T;k_1,\omega\right)dx_3 \tag{C.1}$$

of the gust component of the streamwise Fourier transform $\bar{\bar{G}}^{(0)}\left(\boldsymbol{y}_T\,|\,\boldsymbol{x}_T;k_1,\omega\right)$ of the reduced Green's function $\bar{\bar{G}}\left(\boldsymbol{y}_T\,|\,\boldsymbol{x};k_1,\omega\right)$ is expected to be independent of y_3 and therefore determined by

$$\left[\frac{d^2}{dy_2^2}+\left(k_\infty^2-k_1^2-k_3^2\right)\right]\tilde{C}\quad\left(\quad\quad:\omega,k_1,k_3\right)=\frac{k_\infty^2}{(2\pi)^3}\delta\left(y_2-x_2\right) \tag{C.2}$$

in the outer region where $\sqrt{k_\infty^2-k_1^2}\,y_T,\sqrt{k_\infty^2-k_1^2}\,x_T=O(1)$ when $\bar{\bar{G}}^{(0)}\left(\boldsymbol{y}_T\,|\,\boldsymbol{x}_T;k_1,\omega\right)$ depends on x_3,y_3 only in the combination x_3-y_3 (which we will show to be the case in the low frequency limit) and is therefore given by (Goldstein 1976, p.282)

$$\tilde{C}\quad\left(\quad\quad:\omega,k_1,k_3\right)=H\left(y_2x_2\right)\frac{e^{-\sqrt{k_1^2+k_3^2-k_\infty^2}|x_2|}k_\infty^2w_2\left(y_2,k_3,k_1\right)}{\Delta\left(k_1,k_3\right)} \tag{C.3}$$

for $|x_2|>|y_2|$, where H denotes the Heaviside function

$$w_2\left(y_2,k_3,k_1\right)=e^{-\sqrt{k_1^2+k_3^2-k_\infty^2}|y_2|}+be^{\sqrt{k_1^2+k_3^2-k_\infty^2}|y_2|}, \tag{C.4}$$

b Is an $O(1)$ constant and it follows from Abel's theorem that

$$\Delta\left(k_1\right)=-2\left(2\pi\right)^3 b\sqrt{k_1^2+k_3^2-k_\infty^2}. \tag{C.5}$$

For simplicity, we only consider the symmetric case (which is usually the case of principal interest). The outer solution $\overline{\overline{\overline{G}}}^{(0)}\left(y_2,y_3\mid x_2:\omega,k_1,k_3\right)+\overline{\overline{\overline{G}}}^{(0)}\left(y_2,y_3\mid x_2:\omega,k_1,-k_3\right)$ (where $\overline{\overline{\overline{G}}}^{(0)}\left(y_2,y_3\mid x_2:\omega,k_1,k_3\right)\equiv\overline{\overline{\overline{G}}}^{(0)}\left(u\left(y_2,y_3\right),v\left(y_2,y_3\right)\mid x_2:\omega,k_1,k_3\right)$ see (5.8)) must then behave like

$$\overline{\overline{\overline{G}}}^{(0)}\left(y_2,y_3\mid x_2:\omega,k_1,k_3\right)+\overline{\overline{\overline{G}}}^{(0)}\left(y_2,y_3\mid x_2:\omega,k_1,-k_3\right)=e^{-ik_3y_3}\tilde{C}\quad\left(\cdots:\omega,k_1,k_3\right)$$

$$+e^{ik_3y_3}\tilde{C}\quad\left(\cdots,k_1,k_3\right)\quad\left(\cdots\right)\quad\left(\cdots,k_1,k_3\right)$$

$$=2\tilde{C}\quad\left(\cdots:\omega,k_1,k_3\right)+O\left(k_3y_3\right)^2,\ \text{as}\ k_3y_3\to0 \tag{C.6}$$

since equations(C.3)-(C.5)show that

$$\tilde{C}\quad\left(\cdots,k_3\right)\quad\tilde{C}\quad\left(\cdots,k_3\right). \tag{C.7}$$

And it, therefore, follows that the inner limit of the outer symmetric part of the Fourier-transformed Green's function is

$$\overline{\overline{\overline{G}}}^{(0)}\left(y_2,y_3\mid x_2:\omega,k_1,k_3\right)+\overline{\overline{\overline{G}}}^{(0)}\left(y_2,y_3\mid x_2:\omega,k_1,-k_3\right)\to\frac{-k_\infty^2e^{-\sqrt{k_1^2+k_3^2-k_\infty^2}|x_2|}}{\left(2\pi\right)^3b\sqrt{k_1^2+k_3^2-k_\infty^2}}H\left(y_2x_2\right)$$

$$\times\left\{\left[\left(1+b\right)+\left(b-1\right)\sqrt{k_1^2+k_3^2-k_\infty^2}\,|y_2|\right]+O\left(y_2^2\left(k_1^2+k_3^2-k_\infty^2\right)\right)\right\},\ \text{as}\ \ y_2\sqrt{k_1^2+k_3^2-k_\infty^2}\to0. \tag{C.8}$$

This result will satisfy the wall boundary condition in the outer region where $k_3y_3=O(1)$ if we set $b=1$.

When $\boldsymbol{y}_T$ is in the inner region and $\boldsymbol{x}_T$ is in the outer region equations(5.11) and (5.12) possess a solution of the form

$$\frac{1}{2}\left[\overline{\overline{\overline{G}}}^{(0)}\left(u,v\mid x_2:\omega,k_1,k_3\right)+\overline{\overline{\overline{G}}}^{(0)}\left(u,v\mid x_2:\omega,k_1,-k_3\right)\right]$$

$$=a_0^{\pm}\left(x_2,k_1,k_3,\omega\right)\left(1+O\left(k_\infty^2\right)\right)\ \ \text{for}\ x_2\gtrless0 \tag{C.9}$$

which is symmetric in k_3 satisfies the spanwise transform of the zero derivative wall boundary condition and will match onto the outer solution (C.6)to within an error of $O\left(k_1^2+k_3^2-k_\infty^2\right)$ in the overlap domain where $u,v\to 0, y_2\sqrt{k_1^2+k_3^2-k_\infty^2},\ k_3y_3\to 0$ if we set $b=1$ and

$$a_0^{\pm}\left(x_2,k_1,k_3,\omega\right)=\frac{-k_\infty^2 e^{\mp\sqrt{k_1^2+k_3^2-k_\infty^2}x_2}}{\left(2\pi\right)^3\sqrt{k_1^2+k_3^2-k_\infty^2}}H\left(x_2y_2\right). \tag{C.10}$$

The lowest-order inner solution for the Fourier transformed Green's function that satisfies the wall boundary condition (2.8) for all values of y_3 and is therefore given by(5.20).

Appendix D The scattered component of the low frequency Fourier transformed Green's function

Equations(5.7),(5.8), (6.1) and (5.15)-(5.17) show that the inner solution for the Fourier transform $\overline{\overline{\overline{G}}}_+^{(s)}\left(u,v\,|\,x_1,x_2:\omega,k_1,k_3\right)$ of the scattered component of the Green's function must be of the form

$$\overline{\overline{\overline{G}}}_+^{(s)}\left(u,v\middle|\,x_1,x_2;k_1,k_3,\omega\right)=\sum_{n=-\infty}^{\infty}e^{inv}\overline{\overline{\mathcal{G}}}_n^{(s)}\left(u\,|\,x_1,x_2:\omega,k_1\right)$$

$$=\sum_{n=-\infty}^{\infty}e^{inv}A_n^{(s)}\left(x_1,x_2;k_1,k_3,\omega\right)\hat{P}_n^{\gtrless}\left(u:\omega,k_1\right), \tag{D.1}$$

where

$$\hat{P}_0^{\gtrless}\left(u\right)=c_0^{\gtrless}+c_1^{\gtrless}\int_0^u\frac{\left[M\left(u\right)k_1/k_\infty-1\right]^2}{c^2\left(u\right)}du. \tag{D.2}$$

and $\hat{P}_n^{\gtrless}\left(u:\omega,k_1\right)$ for $n=\pm1,\pm2,....$ denote specific solutions of(5.16) and (5.17)that behave like

$$\hat{P}_n^{\pm}\left(u:\omega,k_1,k_3\right)\to e^{\pm|n|u}\ \text{ as }\ u\to 0 \tag{D.3}$$

And in order to insure that $\overline{\overline{\overline{G}}}^{(s)}$ behaves like the Fourier transform of the zero mean flow flat plate Green's function in the outer region where $k_3y_3, y_2=O\left(1\right)$ we require that the inner solution (D.1) match onto the outgoing wave outer solution

$$\overline{\overline{\overline{G}}}_+^{(s)}\left(y_2,y_3\,|\,x_1,x_2:\omega,k_1,k_3\right)=A_{\gtrless}^{(s)}\left(x_1,x_2\,|k_1,k_3,k_\infty\right)\hat{P}^{\gtrless}\left(\boldsymbol{y}_T:\omega,k_1,k_3\right)$$

$$+O\left(k_1^2+k_3^2-k_\infty^2\right),\ \text{ for } y_2\gtrless 0 \tag{D.4}$$

where $\overline{\overline{\overline{G}}}_+^{(s)}\left(y_2,y_3\,|\,x_1,x_2:\omega,k_1,k_3\right)\equiv\overline{\overline{\overline{G}}}_+^{(s)}\left(u\left(y_2,y_3\right),v\left(y_2,y_3\right)|x_1,x_2,\omega,k_1,k_3\right)$ and

$$\hat{P}^{\gtrless}\left(\boldsymbol{y}_T:\omega,k_1,k_3\right)=\frac{1}{2}\exp\left(\mp\sqrt{k_1^2+k_3^2-k_\infty^2}\,y_2\right)\left[\exp\left(ik_3y_3\right)+\exp\left(-ik_3y_3\right)\right]+o\left(k_\infty\right) \qquad \text{(D.5)}$$

is an outgoing wave solution of the Helmholtz equation (see (5.19))

$$\mathcal{L}\hat{P}^{\gtrless}\left(\boldsymbol{y}_T:\omega,k_1,k_3\right)=0 \qquad \text{(D.6)}$$

in the outer region where $\sqrt{k_1^2+k_3^2-k_\infty^2}\,y_2,\ k_3y_3=O(1)$. The $\mp$ sign in the exponent comes from the requirement that this solution have outgoing wave behavior as $y_2\to\pm\infty$.

An appropriate choice for $\hat{P}^{\gtrless}\left(\boldsymbol{y}_T:\omega,k_1\right)$ is

$$\hat{P}^{\gtrless}\left(\boldsymbol{y}_T:\omega,k_1,k_3\right)=\frac{1}{2}\exp\left(\mp\sqrt{k_1^2+k_3^2-k_\infty^2}\,y_2\right)\left[\exp\left(ik_3y_3\right)+\exp\left(-ik_3y_3\right)\right]+$$

$$a_{\gtrless}\left(k_1,k_3,k_\infty\right)\pi\sqrt{k_\infty^2-k_1^2}\left[e^{\pm i\varphi}H_1^{(1)}\left(y_T\sqrt{k_\infty^2-k_1^2}\right)+e^{\mp\ \ }H_{-1}\left(y_T\sqrt{k_\infty^2-k_1^2}\right)\right]\ \ y_2\gtrless 0 \qquad \text{(D.7)}$$

where $H_\nu^{(1)}$ denotes the Bessel function of the first kind and $a\left(k_1,k_3,k_\infty\right)$ is a function of the indicated arguments.

It now follows from(D.2), (A.2) and #9.1.8 on p.360 of Abramowitz and Stegun (1964) that the inner limit of the outer solution (D.5) is

$$\hat{P}^{\gtrless}\left(u:\omega,k_1,k_3\right)\to 1\mp\sqrt{k_1^2+k_3^2-k_\infty^2}\,y_2-a_{\gtrless}\left(e^{\pm i\varphi}-e^{\mp\ \ }\right)\frac{?}{y_T}+O\left(k_1^2+k_3^2-k_\infty^2\right)$$

$$\to 1\mp\sqrt{\qquad\qquad}\ \mathcal{R}e\ \frac{2i}{z\qquad\qquad}\mp\sqrt{\qquad\qquad}\ \mathcal{R}e\ \frac{\left(e^{W}+1\right)}{\left(1-e^{\cdot\cdot}\right)}$$

$$\mp\ \ \mathcal{R}e\ \ \sqrt{\qquad\qquad}\ \mathcal{R}e\ \sum_{n=1}^{\infty}\ \ \mp$$

$$+O\left(k_1^2+k_3^2-k_\infty^2\right)\to 1-\sqrt{k_1^2+k_3^2-k_\infty^2}\sum_{n=-\infty}^{\infty}e^{inv\pm|n|u}\mp\qquad\qquad O\left(k_1^2+k_3^2-k_\infty^2\right) \qquad \text{(D.8)}$$

as $\sqrt{k_1^2+k_3^2-k_\infty^2}\,y_2,\ k_3y_3\to 0$. And since it follows from (D.1)-(D.3) that the inner solution behaves like

$$\overline{\overline{\overline{G}}}_+^{(s)}\left(u,v\middle|\,x_1,x_2;k_1,k_3,\omega\right)\to c_0^{\gtrless}+c_1^{\gtrless}u+\sum_{n=-\infty}^{\infty}e^{inv}\,\tilde{\ }_{n\ \ }\left(\cdot\cdot_1,\cdot\cdot_3,\omega\right)e^{\pm|n|u} \qquad \text{(D.9)}$$

as $u,v\to 0$, the inner and outer expansions will only match if

$$c_0^{\gtrless} = 1, \quad c_1^{\gtrless} = \mp \qquad \sqrt{k_1^2 + k_3^2 - k_\infty^2}, \quad n = 0, \pm 1, \pm 2, \qquad \text{(D.10)}$$

It then follows from (D.1) and (D.2)that the Fourier transform of the scattered component of the Green's function is of the form (5.22) .

Acknowledgement

The authors would like to thank Dr Clifford Brown for providing his experimental data and for helpful discussions on its interpretation. Dr. James Bridges provided the photograph in figure 1. This work was supported by the NASA Advanced Air Vehicle Program, Commercial Supersonic Technology (CST) and Advanced Air Transport Technology (AATT) Projects. MZA would like to thank Strathclyde University for financial support from the Chancellor's Fellowship

References

Abreu, L. I., Nogueira, P. A. S., Nilton, M. M. and Cavalieri, A. V. G., 2019 Resolvent analysis applied to acoustic analogies. AIAA Paper # 2019-2402.

Baker. D. J. and Peake, N. Scattering on rotational flows. AIAA Paper # AIAA-2019-2554.

Batchelor, G.K. and Proudman, I., 1954, The effect of rapid distortion of a fluid in turbulent motion, Quarterly Journal of Mechanics and Applied Mathematics, Vol. 7, No. 1 pp. 83 – 103.

Bers, A. 1975 Linear waves and instabilities. *In Plasma Physics* (eds. C. Dewitt & J. Perraud), pp. 113-216. Gordon & Breach.

Bilka, M. J., Kerrian, P., Ross, M.H. and Morris, S. C., 2014, Radiated sound from a circular cylinder in a turbulent shear layer, International Journal of Aeroacoustics, vol. 13, no. 7, pp. 511-532.

Bridges, J. and Brown, C.A. 2005, Validation of the small hot jet rig for jet noise research, AIAA Paper 2005-2846.

Briggs, R. J. 1964 *Electron Stream Interaction with Plasmas.* MIT Press.

Brown, C.A. and Bridges, J., 2006, Small hot jet acoustic rig validation, NASA-TM-2006-214234.

Brown, Clifford A. 2013, Jet-Surface Interaction Test: Far-Field Noise Results, *Journal of Engineering for Gas Turbines and Power*, 135(7):071201-071201-7. doi:10.1115/1.4023605.

Brown, Clifford A., 2015a, An Empirical Jet-Surface Interaction Noise Model with Temperature and Nozzle Aspect Ratio Effects, AIAA 2015-0229.

Brown, Clifford A. 2015b, Empirical Models for the Shielding and Reflection of Jet Mixing Noise by a Surface, AIAA 2015-3128.

Campbell, G. A. and Foster, R. M., 1948, *Fourier Integrals for Practical Applications*, p. 111. #867

D. Van Nostrand Co. Inc., Princeton, New Jersey.

Dennis, D. C. J. and Nickels, T. B. 2008, On the limitations of Taylor's hypothesis in constructing long structures in turbulent boundary layers, J. Fluid Mech. 614:197206.DOI:10.1017/S002211008003352

Ffowcs Williams, J. E. and Hall, L. H. 1970, Aerodynamic sound generation by turbulent flow in the vicinity of a scattering half plane, J. Fluid Mech., 40, 657-670

Goldstein, M.E. 1976, Aeroacoustics McGraw-Hill Book Company.

Goldstein, M.E. 1978a, unsteady vortical and entropic distortions of potential flows round arbitrary obstacles, J. Fluid Mech. 89:433-468

Goldstein, M.E. 1978b, Characteristics of the unsteady motion on transversely sheared mean Flows, J. Fluid Mech. Vol.84, part 2, pp. 305-329.

Goldstein, M.E. 1979a, Turbulence generated by entropy fluctuation with non-uniform mean flows, J. Fluid Mech. 93 (part 2) 209-224.

Goldstein, M.E. 1979b, Scattering and distortion of the unsteady motion on transversely sheared mean Flows, J. Fluid Mech. Vol.91, part 4, pp. 601-632.

Goldstein, M.E., Afsar, M. Z. and Leib, S. J. 2013a, Non-homogeneous rapid distortion theory on transversely sheared mean flows, J. Fluid Mech. Vol.736, pp. 532-569.

Goldstein, M.E., Afsar, M. Z., Leib, S.J 2013b, Structure of Small Amplitude Motion on Transversely Sheared Mean Flows, NASA/TM-2013-217862.

Goldstein, M.E., Leib, S. J. and Afsar, M. Z. 2017, Generalized rapid distortion theory on transversely sheared mean flows with physically realizable upstream boundary conditions: application to the trailing edge problem, J. Fluid Mech. Vol.824, pp. 477-512.

Huete Ruiz de Lira, C. 2010, Turbulence generation by a shock wave interacting with a random density inhomogeneity field, Phys. Scr. T142, 014022.

Huete Ruiz de Lira, C. Velikovich, A. L. and Wouchuk, J. G. 2011, Analytical linear theory for the interaction of a planar shock wave with a two- or three-dimensional random isotropic density field, Phys. Rev. E **83**, 056320.

Huete, C., Wouchuk, J. G. and Velikovich, A. L., 2012 Analytical linear theory for the interaction of a planar shock wave with a two- or three-dimensional random isotropic acoustic wave field, Phys. Rev. E **85**, 026312.Hunt, J. C. R. 1973 A theory of turbulent flow around two dimensional bluff bodies J. Fluid Mech. 61:625-706

Hunt, J.C.R. and Carruthers, D. J., 1990, Rapid distortion theory and the 'problems' of turbulence, J. Fluid Mech., 212, pp. 497-532.

Hunt, J.C.R. 1973, A theory of turbulent flow round two-dimensional bluff bodies, J. Fluid Mech., Vol. 61, , pp. 625-706.

Kovasznay, L. S. G., 1953, Turbulence in supersonic flow, J. Aero Sci. 20, issue number 10pp. 657-674.

Leib, S.J. and Goldstein, M.E., 2011 “Hybrid Source Model for Predicting High-Speed Jet Noise,” *AIAA Journal*, Vol. 49, No. 7, pp.1324-1335.

Lighthill, M. J. 1964, *Fourier analysis and Generalized Functions*, Cambridge University Press.

Lin, C. C. 1953, On Taylor’s hypothesis and the accelerating terms in Navier-Stokes equations, Q. Appl. Maths. Vol. 10, pp. 295-306.

Moore, F. K., 1954, Unsteady oblique interaction of a shock wave with a plane disturbance,

NACS Tech. Rep. 2879.

McKeon, B. J. and Sharma, A. S. 2010 A critical-layer framework for turbulent pipe flow. J. Fluid Mech., Vol. 658, pp. 336-382.

Noble, B. 1958, *Methods Based on the Wiener-Hopf Technique for the Solution of Partial Differential Equations*. Pergamon.

Moffatt, H.K. 1967, The interaction of turbulence with strong wind shear. In colloquium on Atmospheric Turbulence and Radio Wave Propagation (ed. A. M. Yaglom and V. I.Tatarski). pp. 139-156. Nauka, Moscow.

Olsen, W. and Boldman, D. 1979, Trailing edge noise data with comparison to theory, AIAA Paper # AIAA 79-1524.

Orr, W. M., 1907, ‘The stability and instability of the unsteady motions of a perfect liquid and of a viscous liquid,’ Proc. Roy. Irish Acad., **A** 27, 69-138.

Pope, S. 2000, *Turbulent Flows* , 1st Edition, Cambridge University Press.

Ramakrishnan, K., Paliath, U., Pastouchencko, N., Malcevic, I., Pilon, A., Morgenstern, J., Buonanno, M., Martinez, M., Majjigi, M.2018, Evaluation of Low Noise Integration Concepts and Propulsion Technologies for Future Supersonic Civil Transports NASA CR-2018-219936.

Ribner, H. S., 1953, ’Convection of a pattern of vorticity through a shock wave, ‘ NACA Tech.

Rep. 1164.

Ross, M. H. 2009, Radiated sound generated by airfoils in a single stream shear layer, Master’s thesis, University of Notre Dame, Notre Dame IN, April 2009.

Sagaut, P. and Cambon, C. 2018, *Homogeneous Turbulence Dynamics*, 2nd Edition, Springer International Publishing.

Taylor, G.I. 1938, The spectrum of turbulence, Proc. R. Soc. A 164, pp.476-490.

Townsend, A. A. 1976, *The structure of turbulent shear flows*, 2nd edition, Cambridge University Press.

Tufts, A., Wang, K. and Wang, M. 2018, Computational study of sound by airfoil interaction with a turbulent shear layer, AIAA paper # 2018-0757, AIAA Aerospace Sciences meeting, Kissimmee Florida, January 8-12.

Wiener, N. 1938, The use of statistical theory to study turbulence, Proc.5th Int. Congress Appl. Mech. P.356-360.

Wouchuk, J. G., Huete Ruiz de Lira, C. and Velikovich, A. L. 2009, Analytical linear theory for the interaction of a planar shock wave with an isotropic turbulent vorticity field, Phys. Rev. E, **79**, 066315.

Xie, Z., Karimi, M. & Girimaji, S. S. 2017, Small perturbation evolution in compressible Poiseuille flow-velocity interactions and obliqueness effects, *Journal of Fluid Mech.* 814 pp. 249-276.